Numerical modelling of methane oxidation efficiency and coupled water-gas-heat reactive transfer in a sloping landfill cover

Feng, S.; Ng, C. W. W.; Leung, A. K.; Liu, H. W.

Published in:
Waste Management

DOI:
10.1016/j.wasman.2017.04.042

Publication date:
2017

Final version published in Waste Management available via DOI: 10.1016/j.wasman.2017.04.042

Numerical modelling of methane oxidation efficiency and coupled water-gas-heat reactive transfer in a sloping landfill cover

S. Feng, C. W. W. Ng, A.K. Leung and H.W. Liu*

Name: Dr Song Feng
Title: Postdoctoral fellow
Affiliation: Department of Civil and Environmental Engineering, Hong Kong University of Science and Technology
Address: Department of Civil and Environmental Engineering, Hong Kong University of Science and Technology, Clear Water Bay, Kowloon, Hong Kong
E-mail: sfengaa@connect.ust.hk

Name: Dr Charles Wang Wai Ng
Title: Chair Professor of Civil and Environmental Engineering
Affiliation: Department of Civil and Environmental Engineering, Hong Kong University of Science and Technology
Address: Department of Civil and Environmental Engineering, Hong Kong University of Science and Technology, Clear Water Bay, Kowloon, Hong Kong
E-mail: cecwwng@ust.hk

Name: Dr Anthony K. Leung
Title: Senior lecturer in Civil Engineering
Affiliation: School of Science and Engineering, University of Dundee
Address: Fulton Building, University of Dundee, Nethergate, Dundee, Scotland, UK DD1 4HN
E-mail: a.leung@dundee.ac.uk

Name: Ms Hong Wei Liu* (Corresponding author)
Title: Doctoral research student
Affiliation: Department of Civil and Environmental Engineering, Hong Kong University of Science and Technology
Address: Department of Civil and Environmental Engineering, Hong Kong University of Science and Technology, Clear Water Bay, Kowloon, Hong Kong
E-mail: hliuan@ust.hk **Tel:** +852 6849 4779

Abstract

Microbial aerobic methane oxidation in unsaturated landfill cover involves coupled water, gas and heat reactive transfer. The coupled process is complex and its influence on methane oxidation efficiency is not clear, especially in steep covers where spatial variations of water, gas and heat are significant. In this study, two-dimensional finite element numerical simulations were carried out to evaluate the performance of unsaturated sloping cover. The numerical model was calibrated using a set of flume model test data, and was then subsequently used for parametric study. A new method that considers transient changes of methane concentration during the estimation of the methane oxidation efficiency was proposed and compared against existing methods. It was found that a steeper cover had a lower oxidation efficiency due to enhanced downslope water flow, during which desaturation of soil promoted gas transport and hence landfill gas emission. This effect was magnified as the cover angle and landfill gas generation rate at the bottom of the cover increased. Assuming the steady-state methane concentration in a cover would result in a non-conservative overestimation of oxidation efficiency, especially when a steep cover was subjected to rainfall infiltration. By considering the transient methane concentration, the newly-modified method can give a more accurate oxidation efficiency.

Key words: Methane oxidation; Reactive transport; Coupled water-gas-heat; Sloping landfill cover

1. Introduction

Methanotrophic microorganisms existed in landfill cover has been utilized to reduce the emission of methane (Scheutz et al., 2009; Czepiel et al., 1996). This biological reaction is considered to be a cost-effective method for mitigating methane emission, especially for small or/and old landfill, where installing a gas collection system may not be financially viable due to relative low methane gas generated. Microbial aerobic methane oxidation involves complex multi-physical processes in relation to coupled water-gas-heat transfer and microbial biochemical activities in unsaturated soil (Czepiel et al., 1996; Ng et al., 2015). Methane oxidation has been revealed to be significantly affected by the temperature and water content in soil (Abichou et al., 2011; Scheutz et al., 2009). Despite wide application of the use of microorganism to control methane emission, the mechanisms involved in the coupled bio-chemo-hydro-thermal processes are not clear. Although various numerical models that consider methane oxidation have been developed, most of them focused on the transfer of different gases only and ignored the effects of water and heat transfer (Stein et al., 2001; Molins et al., 2008; De Visscher and Cleemput, 2003; Yuan et al., 2009). While there exists a limited number of models that incorporated water and heat transfer, the effects of water and temperature on the microbial activity were generally neglected (Garg and Achari, 2010; Hettiarachchi et al., 2007).

To simplify methane oxidation, one-dimensional (1-D) numerical process has been

conducted (Garg and Achari, 2010; Hettiarachchi et al., 2007; Yuan et al., 2009; Spokas et al., 2011; Abichou et al., 2015). The 1-D assumption is valid only for the case of flat landfill covers, but it is not possible to study the two-dimensional (2-D) process involved in the sloping side of a landfill cover. This is because the 2-D spatial distribution of soil water content could potentially lead to variations of gas and heat transfer and methane oxidation rate, due to the coupled processes involved in the soil. The field measurements reported by Di Trapani et al. (2013) and Geck et al. (2016) show that methane emission in the upslope of a sloping cover is higher than that in the downslope. Unfortunately, any corresponding variations of soil water content and soil temperature with time were not measured. Hence, any interrelationship between the coupled water-gas-heat transfer and methane oxidation are not clear (Di Trapani et al. (2013); Geck et al. (2016); Garg and Achari, 2010; Hettiarachchi et al., 2007). More investigations are needed to reveal the underlying mechanisms involved in the microbial methane oxidation and its efficiency in a sloping cover, especially when different cover angles are considered (Di Trapani et al. 2013; Geck et al. 2016).

This study aims to investigate the methane oxidation efficiency in a sloping unsaturated landfill cover through 2-D numerical simulations. A fully coupled model, which can consider water-gas-heat reactive transfer during the biochemical reaction of methane oxidation in unsaturated soil (Ng et al. 2015), was adopted. The model was implemented in the finite-element based, multi-physics software COMSOL

(COMSOL 5.2, 2015). The numerical model and input parameters were calibrated against a set of 2-D flume model tests that quantified methane oxidation (Berger et al., 2005; Berger, 2008) by comparing the computed results with measurements. Once calibrated, the same set of input parameters were used to carry out parametric study. This aims to identify critical factors that could affect the methane oxidation efficiency, including the angle of cover, rainfall intensity and landfill gas generation rate. A new method that considers transient changes of methane concentration during the estimation of the methane oxidation efficiency was proposed and compared against existing methods.

2. Methods

2.1 Theoretical model

The theoretical model includes the governing equations for 2-D transport of water, heat and gases of nitrogen (N_2), oxygen (O_2), carbon dioxide (CO_2) and methane (CH_4), by coupling the principles of mass conservation, energy conservation and fluid transport. Detailed model development is given in Ng et al. (2015).

2.1.1 Water transfer

According to water mass balance, water transfer can be modeled using Richards' equation (Richards, 1931) considering water generation by methane oxidation:

$$\rho_w \frac{\partial \theta_w}{\partial t} = -\nabla(\rho_w v_w) + \rho_{DB} M_{H_2O} r_w \quad (1)$$

where ρ_w is water density; θ_w, ρ_{DB} and M_{H_2O} is volumetric water content, soil dry density and water molar mass, respectively; v_w is water flow velocity; r_w is water generation rate per unit mass of dry soil; and t is time. The physical meaning of Eq. (1) is that the soil water content change ($\rho_w \frac{\partial \theta_w}{\partial t}$) is caused by the net water influx ($-\nabla(\rho_w v_w)$) and water generation ($\rho_{DB} M_{H_2O} r_w$) by methane oxidation.

Non-isothermal water flow (v_w in Eq. (1)) in unsaturated soil is described by Darcy's law as follows (Childs, 1969):

$$v_w = -k_w \left(\nabla \frac{P_w}{\rho_w g} + 1 \right) \tag{2}$$

where k_w is water permeability function; P_w is water pressure; ρ_w is the specific weight of water; and g is gravity acceleration.

2.1.2 Multi-component gas transfer

Considering the principle of mass conservation for gas k (Molins and Mayer 2007):

$$\frac{\partial}{\partial t}[(1-S_w)\phi c_g^k + S_w \phi c_w^k] = -\nabla[v_g c_g^k] - \nabla[v_w c_w^k] - \nabla N_g^k \pm \rho_{DB} r_g^k \tag{3}$$

where ϕ and S_w is soil porosity and degree of saturation, respectively; c_g^k is molar concentration of gas k; c_w^k is molar concentration of gas k dissolved in water; v_g and N_g^k are advective velocity of the gas mixture and the diffusive flux of gas k in the gaseous phase, respectively; r_g^k is reaction rate per unit of dry soil mass for gas k. Eq. (3) considers that the transfer mechanisms of each gas component include (i) advection in the gaseous phase; (ii) advection of the dissolved gas k in water and (iii) gas diffusion in the gaseous phase. In Eq. (3), r_g^k is a function of soil temperature

(details given later). S_w, v_g and N_g^k are also affected by soil temperature through the thermal effects on soil water characteristic curve, permeability function and diffusion coefficient, respectively (Ng et al, 2015).

In Eq. (3), the molar concentration of gas *k* dissolved in water (c_w^k) can be described by Henry's law (Reid et al., 1987)

$$c_w^k = H_g^k c_g^k \tag{4}$$

where H_g^k is Henry's coefficient (*dimensionless*) for gas *k*.

Ignoring gravitational effects, advective velocity for the gas mixture v_g in unsaturated soil can be described by Darcy's law (Parker, 1989):

$$v_g = -k_g \nabla \frac{P_g}{\rho_g g} \tag{5}$$

where P_g is gas pressure; k_g is gas permeability function; and ρ_g is gas density and can be determined by:

$$\rho_g = \sum_{k=1}^{4} c_g^k M_g^k \tag{6}$$

where M_g^k is molar mass of gas *k*. In this study, the molar masses of O_2, N_2, CO_2 and CH_4 are considered to be $3.2*10^{-2}$ *kg/mol*, $2.8*10^{-2}$ *kg/mol*, $4.4*10^{-2}$ *kg/mol* and $1.6*10^{-2}$ *kg/mol*, respectively (Reid et al., 1987).

By Dalton's law and the ideal gas law (Reid et al., 1987),

$$P_g = \sum_{k=1}^{4} c_g^k R(T + 273.15) \tag{7}$$

where *R* is the ideal gas constant (8.314 $J{\cdot}K^{-1}{\cdot}mol^{-1}$).

The diffusive flux N_g^k can be described as follows (Bird et al., 1960):

$$N_g^k = -D_s^k \nabla c_g^k \tag{8}$$

where D_s^k is diffusion coefficient of gas *k* in the gas mixture through soil, which is mainly affected by gas concentration and soil water content (see Eqs. (S1)-(S3) in the supplementary document).

2.1.3 Heat transfer

Using a similar approach adopted by Thomas and Ferguson (1999), invoking the principle of energy balance yields

$$\frac{\partial[E(T-T_r)]}{\partial t} = -\nabla(-\lambda_T \nabla T + Q_{conv}) + Q_{oxi} \tag{9}$$

where T_r and T are reference temperature (room temperature 22 ^{0}C) and soil temperature, respectively; E is heat capacity of the soil at T_r; and λ_T is thermal conductivity of soil. The heat transfer mechanisms considered in Eq. (9) include heat conduction ($-\lambda_T \nabla T$), heat convection (Q_{conv}) and heat generation by methane oxidation (Q_{oxi}).

According to Thomas and Ferguson (1999), the heat capacity of soil at the reference temperature *E* can be defined as follows:

$$E = (1-\phi)\rho_s H_s + \phi S_w \rho_w H_w + \phi S_g \sum_{k=1}^{4} M_g^k c_g^k H_{g,k} \tag{10}$$

where H_s, H_w and $H_{g,k}$ correspond to the specific heat capacities of soil particles, water and gas *k*, respectively; and ρ_s is soil particle density.

Heat convection per unit area Q_{conv} represents the heat transfer by water and gas advection and it can be determined as follows:

$$Q_{conv} = (H_w \rho_w v_w + v_g \sum_{i=1}^{4} c_g^i H_{g,i})(T - T_r) \quad (11)$$

2.1.4 Microbial aerobic methane oxidation

Microbial aerobic methane oxidation may be described by the relationship proposed by Chanton et al. (2009) as follows:

$$CH_4 + (2-x)O_2 \rightarrow (1-x)CO_2 + (2-x)H_2O + x\text{—}CH_2O\text{—} + \text{heat} \quad (12)$$

where —CH_2O— is biomass of methanotrophic microorganisms; x is stoichiometric coefficient, which is taken to be 0.5 in this study (De Visscher et al., 2003) by considering 50% incorporation of carbon into biomass. The heat generated by a mole of methane oxidation is taken to be 632 kJ (Garg and Achari, 2010).

According to the dual-substrate Michaelis–Menten kinetics (Abichou et al., 2011), the methane oxidation rate $r_g^{CH_4}$ in Eq. (3) may be expressed as follows:

$$r_g^{CH_4} = -f_{V,T} f_{V,m} \frac{V_{\max} y_{CH_4}}{K_m + y_{CH_4}} \cdot \frac{y_{O_2}}{K_{O_2} + y_{O_2}} \quad (13)$$

where $V_{\max}$ is the maximum methane oxidation rate per unit of dry soil mass; Ko_2 and K_m are half saturation constants for O_2 and CH_4, respectively; y_{O_2} and y_{CH_4} are molar fractions of O_2 and CH_4, respectively; $f_{V,T}$ and $f_{V,m}$ describe the effects of soil temperature and soil water content on microbial activity, respectively. Detailed equations for $f_{V,T}$ and $f_{V,m}$ are listed in the supplementary document (Eqs. (S4)

and (S5) respectively). Eqs. (1), (3), (9), (12) and (13) which describe the multi-physical processes are all expressed in 2-D form and were solved simultaneously using the finite-element software, COMSOL (COMSOL 5.2, 2015).

2.2 Interpretation methods of methane oxidation efficiency

There are three possible ways to quantify methane oxidation efficiency. The first method is the conventional approach, which bases on the difference between CH_4 influx and outflux under a steady-state condition (De Visscher et al., 1999):

$$\eta_{oxi,t}=\frac{\Gamma^{in}_{CH_4,t}-\Gamma^{out}_{CH_4,t}}{\Gamma^{in}_{CH_4,t}}\times 100\% \tag{14}$$

where $\Gamma^{in}_{CH_4,t}$ and $\Gamma^{out}_{CH_4,t}$ are methane influx and outflux at the bottom and surface of a cover at time *t*, respectively; and $\eta_{oxi,t}$ is methane oxidation efficiency at time *t*.

A new method of interpretation (i.e., the second method) is to consider changes in CH_4 concentration in soil and hence methane oxidation efficiency at transient state (i.e., during rainfall). The conventional method in Eq. (14) may be modified as follows:

$$\eta_{oxi,t2}=\frac{\int_{t1}^{t2}(\Gamma^{in}_{CH_4,t}-\Gamma^{out}_{CH_4,t}-\frac{dS_t}{dt})\,dt}{\int_{t1}^{t2}\Gamma^{in}_{CH_4,t}\,dt}\times 100\% \tag{15}$$

where η_{oxi,t_2} is methane oxidation efficiency at time t_2; and S_t is storage of CH_4 in soil at time *t*, which can be determined by integrating the methane concentration (as obtained from Eq. (3)) over the domain of a problem considered:

$$S_t = \iiint [(1-S_w)\phi c_{g,t}^{CH_4} + S_w \phi c_{w,t}^{CH_4}]dxdydz \quad (16)$$

where $c_{g,t}^{CH_4}$ and $c_{w,t}^{CH_4}$ is molar concentration of CH_4 in gas phase and dissolved in water at time *t*, respectively; x and y are the horizontal and vertical coordinates, respectively; and z is the coordinate perpendicular to x-y plan. Due to low solubility for CH_4 (as shown in Table 1), the dissolved CH_4 ($S_w \phi c_{w,t}^{CH_4}$ in Eq. (16)) can be reasonably ignored. For 2–D analysis, it is assumed that the water-gas-heat transport is identical in any cross-section in any x-y plane. Hence, Eq. (16) can be further simplified as

$$S_t = z_0 \iint [(1-S_w)\phi c_{g,t}^{CH_4} + S_w \phi c_{w,t}^{CH_4}]dxdy \quad (17)$$

where z_0 is the thickness of compacted soil in the z direction.

Eq. (15) may then be approximated to:

$$\eta_{oxi,t_2} = \frac{0.5(t_2 - t_1)[(\Gamma_{CH_4,t_1}^{in} + \Gamma_{CH_4,t_2}^{in}) - (\Gamma_{CH_4,t_1}^{out} + \Gamma_{CH_4,t_2}^{out})] - (S_{t_2} - S_{t_1})}{0.5(t_2 - t_1)(\Gamma_{CH_4,t_1}^{in} + \Gamma_{CH_4,t_2}^{in})} \times 100\% \quad (18)$$

where t_1 and t_2 refer to elapse times ($t_2 > t_1$); Γ_{CH_4,t_1}^{in} and Γ_{CH_4,t_2}^{in} refer to integrated CH_4 influx from the bottom of a cover at t_1 and t_2, respectively; Γ_{CH_4,t_1}^{out} and Γ_{CH_4,t_2}^{out} refer to integrated outflux of CH_4 from the surface of the cover at t_1 and t_2, respectively; and S_{t_1} and S_{t_2} are storage of CH_4 in soil at t_1 and t_2, respectively. The first term in the numerator of Eq. (18) represents the net methane influx during a time interval of ($t_2 - t_1$), while the second term represents any change of CH_4 storage during a time interval of ($t_2 - t_1$).

In the model proposed by Ng et al. (2015), the methane oxidation rate can be determined explicitly through Eq. (13). In the third method of interpretation, the oxidation efficiency may be calculated by integrating the sink term for methane oxidation ($\rho_{DB} r_g^{CH_4}$ in Eq. (3)) over the domain of a problem considered:

$$\eta_{oxi,t} = \frac{\iiint \rho_{DB} r_{g,t}^{CH_4} dxdydz}{\Gamma_{CH_4,t}^{in}} \times 100\% \quad (19)$$

where $r_{g,t}^{CH_4}$ is methane oxidation rate per unit of dry soil mass at time *t*. This alternative method is directly related to methane oxidation. Hence, the efficiency calculated by this method is referred to as a theoretical value. Unless otherwise stated, this method is used to calculate the methane oxidation efficiency. Comparison of the oxidation efficiency determined by these three methods is discussed later.

2.3 Model calibration

2.3.1 Selected case study

The numerical model was calibrated based on published data from flume tests that simulated methane oxidation (Berger et al., 2005). All measured data of these flume tests were reported in Berger (2008). Fig. 1 shows the setup of the flume model. The thickness of the flume and compacted soil perpendicular to the plane are 0.8m and 0.55 m, respectively. The model consists of four soil layers from the top to the bottom, namely, a 300-mm layer of mix sand and compost, a 900-mm layer of loamy sand, a 300-mm layer of silty sand (i.e., referred to as capillary barrier layer) and a 100-mm layer of gravel. The flume angle is 5º (i.e., ~1:11). The side walls of the flume were

thermally insulated. Before testing, the initial soil temperature in the flume was 17.5 ^{o}C, so this temperature was specified at both the top and bottom boundaries. The test was commenced by injecting gases of CH_4 and CO_2 at the same influx rate of 3.62 mol/(m^2 •day) at the bottom of the flume. The applied flux corresponds to a CH_4 generation rate for 4-year decomposed municipal waste (Findikakis et al., 1988). After applying the gas fluxes, the soil was allowed to be stabilized for 19 days, followed by the simulation of summer condition for 45 days (i.e., from Day 19 to 64). During this period, the top and bottom temperatures were controlled to be 20 and 15 ^{o}C, respectively, following the test conditions reported by Berger et al., (2005) and Berger (2008). During the two stages of testing, air was continuously supplied to the surface of the flume. At measurement profiles I and II, any changes in gas concentrations (CO_2, O_2, N_2 and CH_4), volumetric water content (VWC), and temperature were recorded.

2.3.2 Setup of numerical model

Two-dimensional numerical simulations based on the case study presented by Berger (2008) were conducted. Fig. S1 shows the finite element mesh, following exactly the same flume geometry and soil stratification. The top surface boundary AB was specified as zero water flux. At this boundary, the gas molar concentrations (c_g; see Eq. (3)) for CO_2, CH_4, O_2 and N_2 were fixed to be 0.014, 0, 8.6 and 32.53 mol/m^3, respectively, based on the values found from the atmosphere. At the bottom boundary

GF, no transfer was allowed for water, N_2 and O_2, while a constant influx rate of 3.62 mol/(m^2 •day) was applied to simulate the CH_4 and CO_2 injection in the experiment. The side boundaries AG and BF were set to not allow for water, gas (CH_4, CO_2, O_2 and N_2) and heat transfer. At stabilization stage (i.e., from Days 0 to 19), a constant temperature of 17.5 ^oC was specified to both the top and bottom boundaries. During the simulation of summer event from Days 19 to 64, the temperature at the top boundary increased to 20 ^oC, while that at the bottom boundary reduced to 15 ^oC.

The initial conditions of soils in the numerical model followed the measurements made by Berger (2008) before the commencement of the flume testing. The initial VWC in the numerical model was set to be 17.5%, 22%, 15.5% and 4% for the sand-compost mixture, loamy sand, silty sand and gravel, respectively. The initial molar concentration of each gas component was specified to be the same as that found in the atmosphere. The initial soil temperature was 17.5 ^oC.

Porosity values for all the soil materials involved in the model tests presented by Berger (2008) are given in Table 1. The density of liquid water and soil are also summarized in the table. Particle size distributions for each soil layer are shown in Fig. S2. Soil water characteristic curves (SWCCs) for each type of soil (Fig. S3(a)) were obtained from literature and were input to the model. The water permeability functions (Fig. S3(b)) and gas permeability functions (Fig. S3(c)) were estimated

from SWCCs based on the methods proposed by van Genuchten (1980) and Parker (1989), respectively. Henry's constant for each gas component was adopted based on reported values at temperature of 20 ^{o}C by Nastev et al. (1998). Berger et al., (2005) reported that the concentrations of CH_4 and CO_2 were different from those found in the air. Hence, binary diffusion coefficient for each gas component was used in the simulation (via Eq. (S2)). These coefficients (see Table 1) were thus different from the diffusion coefficients in air. Other input parameters including the soil thermal properties as well as the solubility of each gas component are summarized in Table 1. Note that any thermal effects on the soil and gas properties were ignored because of the relatively small range of temperature fluctuation (< 10 ^{o}C) considered in the flume test.

After setting up the numerical model, the analysis was started by firstly simulating the stabilization period between Days 1 and 19. A constant temperature of 17.5 ^{o}C was specified at the top surface and bottom boundaries. Then, during Days 19 and 20, the temperature at the top boundary AB increased linearly from 17.5 to 20 ^{o}C, but that at the bottom boundary reduced from 17.5 to 15 ^{o}C. Finally, from Days 21 to 64, the summer event was simulated by maintaining a constant temperature of 20 ^{o}C at the top surface and 15 ^{o}C at the bottom.

3 Results

3.1 Calibration results

Computed 2-D contours of VWC, temperature and gas concentration (%) of different gases are shown in Figs S4 to S6 in the supplementary document. In the following discussion, only the computed results at profiles I and II are reported to make direct comparison with the measured results.

3.1.1 Verification of computed volumetric water content

Fig. 2(a) compares the measured and computed VWCs along profile I on Day 56, when the measured data were given by Berger (2008). For the following discussion, all the comparisons are made on Day 56, unless otherwise stated. It can be seen that the computed VWC in the 2nd soil layer was generally close to the measurements, with a slight overestimation of about 4% in the 1st layer. The measured lower VWC in the experiment was likely attributed to surface evaporation, which was however neglected in the simulation. Below the depth of 1.2 m in the 3rd soil layer, the simulation showed an increase in VWC, while the VWC remained almost unchanged in the underlying layer. This is attributable to the capillary effect between the 3rd and 4th soil layer. This capillary effect is caused by the contrast of the soil water-entry value (i.e., the suction below which soil water content increases significantly) and saturated permeability (Rahardjo et al., 2013). As a result, soil moisture accumulated in the 3rd layer. As shown in Fig. S3(a), the water-entry values (estimated from the

inflection point on the SWCC) of the 3rd layer is significantly higher than that of the 4th layer. Fig. S3(b) shows that the saturated permeability of the gravel in the 4th layer was almost three orders of magnitude higher than that of the silty sand in the 3rd layer. When water generation by methane oxidation was ignored (i.e., by setting the term $\rho_{DB} M_{H_2O} r_w$ in Eq. (1) to be zero), the VWC profile was about 2% lower than the case with due consideration. This means that the observed change in VWC was largely affected by the hydraulic gradient within the cover soil, rather than the water generation by methane oxidation.

The comparisons of measured and computed VWCs along profile II are depicted in Fig. 2(b). There was a reasonable agreement between the measurements and the simulations. By comparing the results in Figs 2(a) and (b), the VWC profile within the top two soil layers is similar between profiles I and II, suggesting that the cover angle being tested in the flume (i.e., 5 degrees) seems to be too small to cause significant change in VWC. In contrast, a relatively significant increase in VWC is observed in the 3rd layer (i.e., the capillary barrier layer) in downstream (i.e., profile II). This is the consequent of the capillary effect, where the accumulation of soil water in the 3rd layer led to significant lateral water drainage on top of the 4th layer. In contrast, due to the similarities of the SWCCs and permeability functions between the top two layers (Figs. S3(a)and S3(b)), no capillary effect occurred. Soil water thus predominantly seeped in the downward direction due to the relatively small cover angle.

3.1.2 Verification of computed soil temperature

Fig. 3(a) compares the measured and computed soil temperatures along profile I. The measured and computed results are generally consistent. Both the measured and computed temperatures peaked at the interface between the 1st and 2nd soil layers at about 0.3 m depth, where the temperature was about 8 °C higher than the initial value. This is attributable to the heat generation caused by methane oxidation (Q_{oxi} in Eq. (9)). Within the top 0.3 m depth where methane oxidation took place, the VWC at 0.3 m depth was the highest (see Fig. 2(a)), hence resulting in maximum heat dissipation rate (due to thermal conductivity increases as VWC increases (refer to Table 1)). Thus it can be deduced that the maximum methane oxidation occurred at about 0.3 m depth. The comparison implies that in order to maximize the rate of methane oxidation in shallow depths, the thermal properties of a cover may be improved by, for example, increasing the organic content (i.e., compost) of soil. It has been shown that an increase in soil organic content could increase the heat capacity and simultaneously reduce the thermal conductivity (Abu-Hamdeh and Reeder, 2000). In this way, soil temperature in the top part of the cover might be better preserved and less affected by the temperature fluctuation in the atmosphere.

It can be seen in Fig. 3(b) that the measured peak soil temperature on profile II was about 3 °C lower than that for profile I. However, the computed results showed almost

the same soil temperature between profiles I and II. In the simulation, the VWC in the capillary barrier layer (i.e, the 3rd layer) in profile I (Fig. 2(a)) was less than that in profile II (Fig. 2(b)). This thus resulted in upslope flow of landfill gas, providing more "food" (i.e, CH_4) for the bacteria in profile I to undergo a higher rate of methane oxidation and hence inducing higher soil temperature. The observed discrepancy between the measurements and the simulations is probably because of the assumption of constant maximum oxidation rate made in the analysis (refer to Eq. (13)). Due to the assumption made, spatial variation of the maximum methane oxidation rate was not considered in the simulation. However, the assumption made is deemed acceptable, given the small difference between the computed and measured temperature (i.e., < 3 ^oC).

3.1.3 Verification of computed gas concentrations

Fig. 4(a) shows the concentrations for O_2, CO_2, CH_4 and N_2 along profile I. The measurements show that the concentrations of O_2 and N_2 in shallower depths increased due to the supply from the atmosphere. Correspondingly, the concentrations of CH_4 and CO_2 near the same depths were diluted. For a given soil depth, the concentration of CO_2 was higher than that of CH_4, although the latter has a higher diffusion coefficient than CO_2 (as shown in Table 1). This is because a portion of CH_4 has been converted to CO_2 during the process of methane oxidation (see Eq. (12)). At about 0.3 m depth, the concentration of CH_4 was close to zero, which suggests that the

oxidation capacity was likely to have exceeded the input methane flux in this particular flume model. In fact, the methane oxidation efficiency measured by Berger et al. (2005) was as high as 95%. Microbial oxidation was therefore effective to reduce CH_4 emission.

In general, the numerical simulation captured the responses of all four gas components reasonably well. There was a slight underestimation of N_2, especially at depths below 0.7 m probably because of some overestimation of VWC (Fig. 2(b)). In profile II (Fig. 4(b)), both measured and computed responses of each gas component were similar to those found in profile I, consistent to the similar VWC distributions observed between profiles I (Fig. 2(a)) and II (Fig. 2 (b)). This further indicates that the relatively gentle angle of cover (i.e., 5 ^oC) does not introduce significant effects on the spatial variation of gas concentration.

3.2 Parametric studies

By using the calibrated numerical model, three series of parametric studies were conducted to improve the understanding of methane oxidation in a sloping landfill cover. Series 1 aims to investigate the effects of the angle of cover (i.e., 0^o, 10^o and 18^o) on the 2-D spatial variation of methane oxidation. The maximum angle of 18^o is based on the maximum slope gradient of 1:3 for cover design given in the guide suggested by Dwyer et al. (2002). In the flume model test (Berger et al., 2005; Berger,

2005), the methane oxidation capacity exceeded the input methane flux. Hence, in this series, a methane flux rate of 11.82 mol/(m^{-2} day^{-1}) was applied, corresponding to a methane generation rate for 3-year old decomposed municipal waste (Findikakis et al., 1988).

The objective of series 2 was to study how the rainfall intensity would affect the methane oxidation efficiency. Three rainfall intensities of 43, 60 and 72 mm/hour were adopted, with consideration of 2 h of rainfall duration. These three rainfall events correspond to return periods of 2-year, 5-year and 10-year, respectively, based on the statistical analyses of 100-year rainfall data obtained from the Hong Kong observatory (Tang and Cheung, 2011). The applied CH_4 gas influx at the base of each flume model was the same as that in the flume model test by Berger et al. (2005).

Series 3 explores the effects of gas generation rate on the oxidation efficiency. A range of landfill gas generation rates (as shown in Table 2 based on Findikakis et al. (1988)) were used to study their effects on oxidation efficiency at cover angles of 0° and 18°. Findikakis et al. (1988) reported that the gas generation rates increased from 7.18 mol/(m^2day) to 11.82 mol/(m^2day) from the 2^{nd} to the 3^{rd} year, but it then dropped to 3.62 mol/(m^2day) in the 4^{th} year due to the reduced rate of bacterial bio-chemical decomposition of the waste (De Gioannis et al., 2009). The analysis plan is summarized in Table 2.

3.2.1 Influence of the cover angle (Series 1)

Fig. 5(a) compares the computed VWC profiles between cover angles of 0^o and 18^o obtained from series 1, considering water generation by methane oxidation. For the flat cover, VWC along profile I was identical to that in profile II, as expected, because the problem was 1-D and did not involve any lateral flow. When the cover angle increased to 18^o, the effects of 2-D water flow became prominent. It can be seen that the VWC in the 2^{nd} soil layer reduced in both profiles I and II. This is because the increased hydraulic gradient in the steeper cover resulted in more significant lateral seepage to the 3^{rd} soil layer, causing an increase in VWC in the capillary barrier layer. Due to the capillary effect, significant downslope lateral water drainage occurred on top of the 4^{th} layer. This hence results in the increase in VWC downstream in profile II. Regardless of the cover angle considered, the changes in VWC along profiles I and II are largely because of water flow due to hydraulic head difference between the upslope and the downslope of the cover soil. Additional analysis without modelling water generation by methane oxidation (Fig. S7) shows that the difference of VWC is less than 2%. This means that for the range of methane flux rate (3.62 –11.82 mol/m^{-2} day^{-1}) considered in this study, the 2-D seepage in the cover soil plays a much more significant role than the water generation by methane oxidation. Significant 2-D spatial variations of gas transfer can also be seen in the steeper cover. Along profile I (Fig. 5(b)), the steeper cover has higher concentrations of CH_4 and CO_2 than those in

the flat cover, but the concentrations of O_2 and N_2 were smaller. The observed increases in CH_4 and CO_2 concentration were because the directions of their diffusive and advective fluxes were both upward. On the contrary, the advective flux of O_2 and N_2 was opposed by the downward diffusive flux due to the concentration gradient between the atmosphere and the shallow cover soil. Along profile II (Fig. 5(c)), an opposite trend is observed. The concentrations of CH_4 and CO_2 in the steeper cover were lower than those found in the flat cover, whereas the concentrations of N_2 were higher. The reason is that in the steeper cover, the VWC along profile I was less than that along profile II (Fig. 5(a)), resulting in a higher gas permeability in the gravel layer. Since the gravel layer has much higher gas permeability (see Fig. S2(c)), significant bypassing of the other wetter soil layers took place. This facilitates gas advection towards the upslope of the cover. In addition, the changes in the concentration of O_2 between profiles I and II were less apparent than that found for N_2 for cover angle of 18^o. It is attributable to the consumption of O_2 by the methane oxidation, while N_2 is assumed as a stagnant gas in this study.

Comparison of soil temperature between the flat and the steep covers is depicted in Fig. 5(d). It can be seen that the temperature difference between profiles I and II at the cover angle of 18° was greater than that found in the flat case. This is because greater methane oxidation occurred at profile II than profile I in the steeper slope (as indicated by the lower concentration of CH_4 at profile II shown in Fig. 5(c)). More

heat was thus released at profile II, hence inducing higher amount of soil temperature.

The effects of cover angle on the methane oxidation efficiency are shown in Fig. 6. During the stabilization stage from Days 1 to 19, the cover angle has no influence on the methane oxidation efficiency. The efficiency increased abruptly in the first few days, because of the temperature increase due to the heat generation through methane oxidation. For example, for covers with different sloping angles, the maximum temperature increases are similar (i.e. about 6 ^{o}C), which resulted in an increase in the rate of methane oxidation by 60% (refer to Eq. (S4)). During the summer period from Days 19 to 20, the efficiency increased instantaneously for all cover angles considered, due to the applied increase in the soil surface temperature from 17.5 to 20 ^{o}C. Thereafter, gentler covers (i.e., with angles of 0 and 5^{o}) almost maintained the oxidation efficiency at about 80%. On the contrary, for steeper covers (i.e., with angles of 10 and 18^{o}), significant drops of efficiency were resulted. This is because the increase in cover angle results in a higher hydraulic gradient, causing more significant desaturation of the cover soil. Hence, this reduced oxidation efficiency, encouraging methane emission. Note that the amount of water generation by methane oxidation, which is affected by the increase in soil temperature, is less than 2% (see Fig. 2). This means that the increase in water permeability due to such an increase in soil water content has minimal effect on the increased downslope water flow in steeper cover.

Fig. 7 shows the rate of methane emissions along the 4.8 m-long cover surface for different cover angles. For the flat cover (i.e., 0°), CH_4 emission was uniform due to 1-D gas flow involved in the soil. As the cover angle increases, there was increased methane emission at the upslope of the cover, while the emission was reduced in the downslope even though CH_4 was supplied at the bottom of flume model uniformly. This is because of the reduction of VWC at the upslope of the cover (see Fig. 5 (a)) due to downslope water flow, which subsequently led to increased gas permeability and diffusivity for methane to emit. This implies that the angle of a cover should be reduced as much as possible to prevent from the reduction of methane oxidation efficiency associated with the 2-D redistribution of soil moisture. The simulation results also reveal the importance of considering 2-D spatial variation of water-gas-heat transfer processes for more correct estimation of methane oxidation and emission that would not be possible using existing 1-D modelling approaches.

3.2.2 Influence of rainfall intensity on methane emission (Series 2)

Fig. 8 shows the effects of the rainfall intensity on the methane emission rate during 2 h of rainfall for the cover angle of 5°. The inset shows that the methane emission initially decreased in the first 50 minutes of rainfall due to the reduction of gas transfer as the soil water content increased. During most of the course of rainfall, the methane emission rate in all cases was almost zero. Closer to the end of rainfall event,

significant CH_4 emission was resulted under 5- and 10-year rainfall. Both of these rates fall within the range of allowable emission rate (0.45 – 3.75 mol/(m^2 •day) recommended by the Australian design guideline (Carbon Farming Initiative, 2013). In contrast, the methane emission rate under the 2-year return rainfall was about one order of magnitude lower than the other cases and was therefore negligible. Moreover, it can be seen that the methane emission occurred earlier when the rainfall intensity was higher. This is because under heavier rainfall condition, there was more significant increase in VWC (see Fig. S8), leading to a greater reduction in gas transfer. The reduced influx of O_2 hence reduced methane oxidation. Furthermore, as methane gas was constantly supplied at the base of the flume, the building up of gas pressure (see Fig. S9) caused increased gas advection. This is consistent with the findings from Zhang et al. (2013), who reported an increase in methane emission after a rainfall event in their landfill site. During rainfall in a landfill site, it is possible for an increase in VWC to lead to lateral transport of methane, causing potential emissions adjacent to the site. A tragic instance was reported at Skellingsted landfill, Denmark, where a heavy rainfall together with a drop in atmospheric pressure resulted in lateral migration of methane, leading to an explosion of a house nearby (Kjeldsen and Fischer, 1995). For the flume model simulated in this study, the lateral boundary was impermeable for gas transfer, and therefore gas emission was allowed only on the surface of the cover.

Fig. 9(a) shows the methane oxidation efficiency estimated by the conventional steady-state method (Eq. (14)). For the 2-year rainfall event, the efficiency almost unchanged and remained at about 100% during the first hour of rainfall. The efficiency then drops to around 90% at the end of the rainfall event. As the rainfall return period increases, the drop of efficiency is more significant, following the trend of methane emission rate shown in Fig. 8. It can also be seen that the higher the rainfall intensity, the earlier the reduction of efficiency occurred and the greater the reduction it would be. When the calculation considered transient change in methane concentration in soil during rainfall (i.e., through Eq. (18)), significant different efficiencies are resulted (see Fig. 9(b)) during the first hour of rainfall. Note that the calculation selected a time interval ($(t_2 - t_1)$ in Eq. (18)) of 360 s. Compared with the results determined by the conventional method, the transient-state method shows much earlier reduction of efficiency after the first 10 min of rainfall. The conventional method has ignored the transient increases in methane concentration in the soil during rainfall (refer to Fig. S10), and this is the reason causing its substantial overestimation of efficiency during the initial stage of the three rainfall events considered. For the 2- and 5-year rainfall events, the transient effects vanish as the duration of rainfall increases. Eventually the efficiency reaches zero, regardless of the method of calculation used.

Since the numerical model can calculate the methane oxidation rate through Eq. (13)

directly, it is therefore possible to use the third interpretation method (i.e., through Eq. (19)) to determine the "theoretical" oxidation efficiency to cross-check the accuracy of the transient method. It can be seen in Fig. 9(c) that the theoretical oxidation efficiency is close to that shown in Fig. 9(b), for the three rainfall events considered. The discrepancies are not surprising due to the mathematical approximation made when determining the net methane influx and methane storage in Eq. (18). The comparison suggests the transient method, which could capture the change in methane concentration during the early stage of a rainfall event, offers a more accurate estimation of methane oxidation efficiency than the conventional steady-state method.

3.2.3 Influence of gas generation rate on methane oxidation efficiency (Series 3)

Fig. 10 shows the effects of the rate of landfill gas generation on the methane oxidation efficiency at cover angles of 0° and 18°. For the flat cover, the efficiency decreased exponentially as the gas generation rate increased. This is expected because the methane input has exceeded the oxidation capacity, which is considered to be constant in Eq. (13). De Visscher et al. (2003) also demonstrated a reduction of methane oxidation efficiency due to an increase in landfill gas generation rate in their 1-D numerical simulation. It can be seen that the reduction of efficiency was much more significant when the landfill gas generation rate increased beyond 7.18 mol/(m^2day) (i.e., corresponding to 2-year decomposed waste). This is because the gas pressure in the cover increased as the landfill gas generation rate increased,

resulting in greater amount of methane emission. As the cover angle increased to 18°, similar reduction trend is resulted, but rate of the reduction of the efficiency is greater. At the peak gas generation rate for the 3-year-old waste, the efficiency drops to 70%, which is 10% lower than that obtained in the flat cover. This is because of the larger methane emission in the upslope of the steeper cover caused by the soil desaturation upon downslope water flow.

4. Discussion

Two major concerns of the design of a landfill cover are upward methane emission to the atmosphere and downward water percolation to the underlying waste. It is well known that a steeper capillary barrier (i.e., the 3rd and 4th soil layers in this study; Fig. 1) would have a longer diversion length (defined as the distance water is diverted laterally with no/negligible downward flow through the fine/coarse interface (Morris and Stormont, 1999). This would hence result in enhanced lateral water drainage along the interface of the 3rd and the 4th layer and subsequently reduced water percolation. However, because of this enhanced seepage in a steep cover, the soil desaturation would consequently result in increased gas permeability and diffusivity, promoting methane emission at the upslope of a cover and hence reducing the methane oxidation efficiency. It is thus crucial for engineer to select an appropriate cover angle for optimizing the design of the cover soil, against both methane emission and water percolation. If a landfill cover is to be constructed in arid to semiarid region

where rainfall infiltration and water percolation might be less important, it would be desirable to design a flatter cover so that the methane oxidation efficiency can be enhanced. In contrast, in humid region, steeper cover would better facilitate lateral water drainage for minimizing water percolation. However, precaution must be paid to control the methane emission as a result of the desaturation of the cover soil. It would be ideal to couple the steeper cover with gas collection or monitoring schemes, especially at the upslope of the cover, where gas emission is the most critical. If for practical reasons the cover angle has to be steep, a possible way to mitigate methane emission is to enhance the water retention capacity of the soil used to construct the capillary barrier (i.e., the 3rd layer in Fig. 1), such as silt. It is because at a given porosity, silt has smaller pore size compared with silty sand used to construct the capillary barrier layer in the flume tests conducted by Berger et al. (2005), leading to larger water retention capacity. This would help minimize the redistribution of soil water content (and hence gas emission) as a result of downslope water flow in the cover during rainfall.

It is important to reveal from this study that using the conventional way to determine the methane oxidation efficiency (Eq. (14)) could be misleading (see Fig. 9(a)), due to the negligence of the possible changes in methane concentration in soil, especially during the early stage of a rainfall event. If possible, post-construction measurement or monitoring of methane concentration profiles in the cover soil is recommended so

that engineer can apply the newly-modified method (Eq. (18)) to more correctly estimate the oxidation efficiency of their design cover. This proposed approach has been shown to produce close oxidation efficiencies with the theoretical values under the 2-, 5- and 10-year rainfall events (compare Figs 9(b) and (c)). Such monitoring can be readily achieved by installing an array of methane concentration sensors in the cover soil. Depending on the steepness of the cover, more than one profile of methane concentration might be needed to capture the spatial variation of methane in the cover due to the coupled water-gas-heat transport. However, if post-construction monitoring is not possible, extra caution should be taken to the application of the conventional method. For short-duration rainfall events, steady-state methane concentration would need to be justified to prevent from non-conservative overestimation of the methane oxidation efficiency.

5. Conclusions

For a given methane oxidation capacity, a steeper cover has a lower methane oxidation efficiency. This is because of significant downslope water flow, during which the soil desaturation in the upslope of the cover would lead to enhanced gas permeability and diffusivity for methane emission. Although a steep cover requires stricter controls of gas emission, the capillary barrier in the steep cover could more effectively reduce water percolation to the waste underneath. A potential way to optimize the reduction of gas emission and water percolation in a steep cover may be

to select soil with high water retention capacity in the capillary barrier.

Parametric study also shows that the methane oxidation efficiency could be reduced significantly with an increase in rainfall intensity. Higher methane emission rate was observed near the end of a 2 h-rainfall event when the return period of the rainfall was higher. This is because the increase in soil water content due to rainfall infiltration reduced gas permeability and diffusivity, which consequently caused a drop of the influx of O_2 from the atmosphere. The reduced O_2 availability hence reduced the methane oxidation in the cover.

Methane oxidation efficiency was found to decrease as the generation rate of methane at the bottom of a cover increased, due to increased gas emission rate predominantly through advection. It is identified that such a reduction was significant in a steeper cover. This is attributed to the enhanced downslope water flow, during which the soil desaturation in the cover promoted upslope gas emission.

This study also reveals that assuming the steady-state methane concentration in a landfill cover could result in non-conservative overestimation of the methane oxidation efficiency during the early stage of a rainfall event. This overestimation was found to be much more significant for landfill covers under transient rainfall conditions, where methane concentration was normally not at the steady state.

However, such overestimation reduced when longer duration of rainfall event was considered. In order to consider the effects of transient methane response during rainfall, an improved determination method was proposed. The calculated oxidation efficiency was close to the theoretical values determined by the validated numerical model. The newly-modified method may be readily used in the field condition as long as methane concentration profiles are monitored in a cover.

Acknowledgements

The authors gratefully acknowledge a research grant (HKUST6/CRF/12R) provided by the Research Grants Council (RGC) of the Hong Kong Special Administrative Region. The third author also acknowledges the EU Marie Curie Career Integration Grant under the project ‘BioEPIC slope’ and research travel support from the Northern Research Partnership (NRP).

References

Abichou, T., Mahieu, K., Chanton, J., Romdhane, M. and Mansouri, I., 2011. Scaling methane oxidation: from laboratory incubation experiments to landfill cover field conditions. Waste Management, 31, 978–986.

Abichou, T., Kormi, T., Yuan, L., Johnson, T. and Francisco, E., 2015. Modeling the effects of vegetation on methane oxidation and emissions through soil landfill final covers across different climates. Waste Management, 36, 230-240.

Abu-Hamdeh, N. H. and Reeder, R. C., 2000. Soil thermal conductivity effects of density, moisture, salt concentration, and organic matter. Soil Science Society of America Journal, 64, 1285-1290.

Albright, W. H., Benson, C. H., Gee, G. W., Roesler, A. C., Abichou, T., Apiwantragoon, P., Lyles, B. F and Rock, S. A., 2004. Field water balance of landfill final covers. Journal of Environmental Quality, 33(6), 2317-2332.

Arthur, E., Cornelis, W. M., Vermang and De Rocker, E., 2011. Amending a loamy sand with three compost types: impact on soil quality. Soil Use and Management, 27(1), 116-123.

Becker, B. R., Misra, A. and Fricke, B. A., 1992. Development of correlations for soil thermal conductivity. International Communications in Heat and Mass Transfer, 19, 59-68.

Berger, J., Fornes, L. V., Ott, C., Jager, J., Wawra, B. and Zanke, U., 2005. Methane oxidation in a landfill cover with capillary barrier. Waste Management, 25(4), 369–373.

Berger, J., 2008. Biological methane oxidation in Landfill. PhD thesis, Darmstadt, Techn. Universität, Germany.

Bird, R. B., Stewart, W. E. and Lightfoot, E. N., 1960. Transport phenomena, John Wiley & Sons.

Carbon Farming Initiative, 2013. Guidelines for calculating regulatory baselines for legacy waste landfill methane projects, Australian Government.

Childs, E. C., 1969. An Introduction to the Physical Basis of Soil Water Phenomena. London: Wiley-Interscience.

COMSOL 5.2, 2015. COMSOL Multiphysics Reference Manual. COMSOL, Inc., Stockholm, Sweden.

Czepiel, P., Mosher, B., Crill, P. and Harriss, R., 1996. Quantifying the effect of oxidation on landfill methane emissions. Journal of Geophysical Research, 101, 16721 – 16729.

Chanton, J. P., Powelson, D. K. and Green, R. B., 2009. Methane oxidation in landfill cover soils, is a 10% default value reasonable? Journal of Environmental Quality, 38, 654–663.

De Gioannis, G., Muntoni, A., Cappai, G. and Milia, S., 2009. Landfill gas generation after mechanical biological treatment of municipal solid waste. Estimation of gas generation rate constants. Waste Management, 29(3), 1026-1034.

De Visscher, A., Thomas, D., Boeckx, P. and Van Cleemput, O., 1999. Methane oxidation in simulated landfill cover soil environments. Environmental Science and Technology, 33, 1854–1859.

De Visscher, A. and Van Cleemput, O., 2003. Simulation model for gas diffusion and methane oxidation in landfill cover soils. Waste Management, 23, 581–591.

Di Trapani, D., Di Bella, G. and Viviani, G., 2013. Uncontrolled methane emissions from a MSW landfill surface: Influence of landfill features and side slopes. Waste Management, 33(10), 2108-2115.

Dwyer, S. F., Bonaparte, R., Daniel, D. E., Koerner, R. M. and Gross, B., 2002. Technical guidance for RCRA/CERCLA final covers. US Environmental Protection Agency, Office of Solid Waste and Emergency Response, Washington, DC, USA.

Ewen, J. and Thomas, H. R., 1987. The thermal probe—a new method and its use on an unsaturated sand. Geotechnique, 37, 91-105.

Fredlund, M. D., Fredlund, D. G. and Wilson, G. W., 1997. Prediction of the soil-water characteristic curve from grain-size distribution and volume-mass properties. In Proc., 3rd Brazilian Symp. on Unsaturated Soils, Rio de Janeiro, 1, 13-23.

Findikakis, A. N., Papelis, C., Halvadakis, C. P. and Leckie, J. O., 1988. Modelling gas production in managed sanitary landfills. Waste Management & Research, 6(1), 115-123.

Garg, A. and Achari, G., 2010. A comprehensive numerical model simulating gas, heat, and moisture transport in sanitary landfills and methane oxidation in final covers. Environmental Modeling & Assessment , 15, 397–410.

Geck, C., Scharff, H., Pfeiffer, E. M. and Gebert, J., 2016. Validation of a simple model to predict the performance of methane oxidation systems, using field data from a large scale biocover test field. Waste Management, 56, 280-289.

Hettiarachchi, V. C., Hettiaratchi, J. P. A. and Mehrotra, A. K., 2007.Comprehensive one-dimensional mathematical model for heat, gas, and moisture transport in methane biofilters. Practice Periodical of Hazardous, Toxic, and Radioactive Waste Management, 11(4), 225-233.

Hillel, D., 1982. Introduction to soil physics (Vol. 364). New York: Academic press, New York.

Kämpf, M., Holfelder, T. and Montenegro, H., 2003. Identification and parameterization of flow processes in artificial capillary barriers. Water Resources Research, 39(10).

Kjeldsen, P. and Fischer, E.V., 1995. Landfill gas migration – Field investigations at Skellingsted landfill, Denmark. Waste Management and Research, 13, 467–484.

Molins, S. and Mayer, K. U., 2007. Coupling between geochemical reactions and multicomponent gas and solute transport in unsaturated media: A reactive transport modeling study. Water Resources Research, 43(5).

Molins, S., Mayer, K. U., Scheutz, C. and Kjeldsen, P., 2008. Transport and reaction processes affecting the attenuation of landfill gas in cover soils. Journal of Environmental Quality, 37(2), 459-468.

Morris, C.E. and Stormont, J.C., 1999. Parametric study of unsaturated drainage layers in a capillary barrier. Journal of Geotechnical and Geoenvironmental Engineering, 125(12), 1057-1065.

Nastev, M., 1998. Modeling landfill gas generation and migration in sanitary landfills and geological formations. PhD Thesis, University of Calgary, Canada.

Ng, C. W. W., Feng, S. and Liu, H. W., 2015. A fully coupled model for water–gas–heat reactive transport with methane oxidation in landfill covers. Science of The Total Environment, 508, 307-319.

Parker, J. C., 1989. Multiphase flow and transport in porous media. Review of Geophysics, 27 311-328.

Rahardjo, H., Satyanaga, A., Harnas, F.R., Wang, J.Y. and Leong, E.C., 2013. Capillary barrier system for landfill capping. International Symposium on Coupled Phenomena in Environmental Geotechnics, Torino, Italy, p.425.

Reid, R. C., Prausnitz, J. M. and Poling, B. E., 1987. The properties of gases and liquids. McGraw-Hill, New York.

Richards, L. A., 1931. Capillary conduction of liquids through porous mediums. Journal of Applied Physics, 1, 318–333.

Scheutz, C., Kjeldsen, P., Bogner, J. E., De Visscher, A., Gebert, J., Hilger, H. A., HumberHumer, M. and Spokas, K., 2009. Microbial methane oxidation

processes and technologies for migration of landfill gas emissions. Waste Management and Research, 27, 409-455.

Spokas, K., Bogner, J. and Chanton, J., 2011. A process-based inventory model for landfill CH4 emissions inclusive of seasonal soil microclimate and CH_4 oxidation. Journal of Geophysical Research: Biogeosciences (2005–2012), 116(G4).

Stein, V. B., Hettiaratchi, J. P. A. and Achari, G., 2001. A numerical model for biological oxidation and migration of methane in soils. ASCE Practice Periodical of Hazardous, Toxic, and Radioactive Waste Management, 5 (4), 225–234.

Stormont, J. C. and Morris, C. E., 1998. Method to estimate water storage capacity of capillary barriers. Journal of Geotechnical and Geoenvironmental Engineering, 124(4), 297-302.

Tang C. S. C. and Cheung S. P. Y., 2011. Frequency Analysis of Extreme Rainfall Values . GEO report No. 261, Geotechnical Engineering Office, Hong Kong.

Thomas, H. R. and Ferguson, W. J., 1999. A fully coupled heat and mass transfer model incorporating contaminant gas transfer in an unsaturated porous medium. Computers and Geotechnics, 24, 65–87.

Van Genuchten, M. T., 1980. A closed form equation for predicting the hydraulic conductivity of unsaturated soils. Soil Science Society of America Journal, 44, 892–898.

Woodside, W. T. and Messmer, J. H., 1961. Thermal conductivity of porous media. I. Unconsolidated sands. Journal of Applied Physics, 32, 1688-1699.

Yuan L., Abichou T., Chanton J., Powelson D.K. and De Visscher A., 2009. Long-term numerical simulation of methane transport and oxidation in compost biofilter. Practice Periodical of Hazardous, Toxic, and Radioactive Waste Management, 13, 196-202.

Zhang, H., Yan, X., Cai, Z. and Zhang, Y., 2013. Effect of rainfall on the diurnal variations of CH_4, CO_2, and N_2O fluxes from a municipal solid waste landfill. Science of the Total Environment, 442, 73-76.

List of figures in the manuscript

List of tables in the manuscript

The supplementary material includes:

Fig. S10 Computed methane concentration distributions during different rainfall intensities: (a) at profile I; and (b) at profile II

Table. 1 Parameters used in the simulation of the flume model test

Parameter		Value	Source
Porosity	Mixture of sand and compost	0.53	Arthur et al. (2011)
	Loamy sand	0.35	Fredlund et al. (1997)
	Silty sand	0.37	Stormont and Morris (1998)
	Gravel	0.34	Kampf et al. (2003)
Soil dry density (kg/m^3)	Mixture of sand and compost	1100	Berger (2005)
	Loamy sand	1700	
	Silty sand	1450	
	Gravel	1716	
Water density (kg/m^3)		1000	Nastev (1998)
Henry's constant (dimensionless)	CO_2	0.8145	
	O_2	0.0318	
	N_2	0.0159	
	CH_4	0.0316	
Binary diffusion coefficient (10^{-6} m^2s^{-1})	O_2 and N_2	2.083	Molins and Mayer (2007)
	CO_2 and N_2	1.649	
	CH_4 and N_2	2.137	
	CO_2 and O_2	1.635	
	O_2 and CH_4	2.263	
	CO_2 and CH_4	1.705	
Thermal conductivity ($Jm^{-1}s^{-1}K^{-1}$)	saturated sand mixed with compost	1.22	Woodside and Messmer (1961)
	dry sand mixed with compost	0.65	
	saturated loamy sand	1.59	Abu-Hamdeh and Reeder (2000)
	dry loamy sand	0.23	
	saturated sand	2.89	Ewen and Thomas (1987)
	dry sand	0.37	
	saturated gravel	2.17	Becker et al. (1992)
	dry gravel	0.40	
Specific heat capacity of ($J\ kg^{-1}K^{-1}$)	soil particle	800	Hillel (1982)
	water	4185	Reid et al. (1987)
	CO_2	816	
	O_2	1005	
	CH_4	2160	
	N_2	930	
Methane oxidation rate ($mol\ kg^{-1}s^{-1}$)		$8.22*10^{-7}$	Berger (2008)
K_{o2}		0.012	De Visscher et al. (1999)
K_{ch4}		0.0066	

Table. 2 Summary of parametric study

Series	Case number	Cover angle (°)	Gas generation rate (mol/(m^{2}day))	Rainfall intensity (mm/hour)[d]	Rainfall duration (hour)
Basic[a]	1	5	3.62[b]	Not applicable	Not applicable
CA[a]	1	0[c]	11.82[b]	Not applicable	Not applicable
	2	10			
	3	18			
RI[a]	1	5	3.62	43	2
	2			60	
	3			72	
GG[a]	1	0, 18	3.62	Not applicable	Not applicable
	2		4.50		
	3		6.00		
	4		7.18[b]		
	6		8.50		
	7		9.50		
	8		10.50		
	9		11.82		

Note:

(a) Duration for Basic, CA (**c**over **a**ngle) and GG (**g**as **g**eneration) series is 56 days. The results of Basic series on day 56 serve as the initial conditions for RI (**r**ainfall **i**ntensity) series.

(b) 3.62 mol/(m^{2}day) is the CH_4 influx applied in test (Berger et al, 2005). 3.62 mol/(m^{2}day) , 7.18 mol/(m^{2}day) and 11.82 mol/(m^{2}day) correspond to CH_4 generation rates for 4-year, 2-year and 3-year decomposed waste (Findikakis et al., 1988), respectively.

(c) For cover angle of 0°, in order to simulate the in-situ flat cover, a rectangular geometry is adopted, which has the same width and height as that of flume model with trapezoidal geometry (Fig. S1).

(d) 10% of rainfall was adopted as surface runoff based on the field measurements of landfill covers presented by Albright et al. (2004).

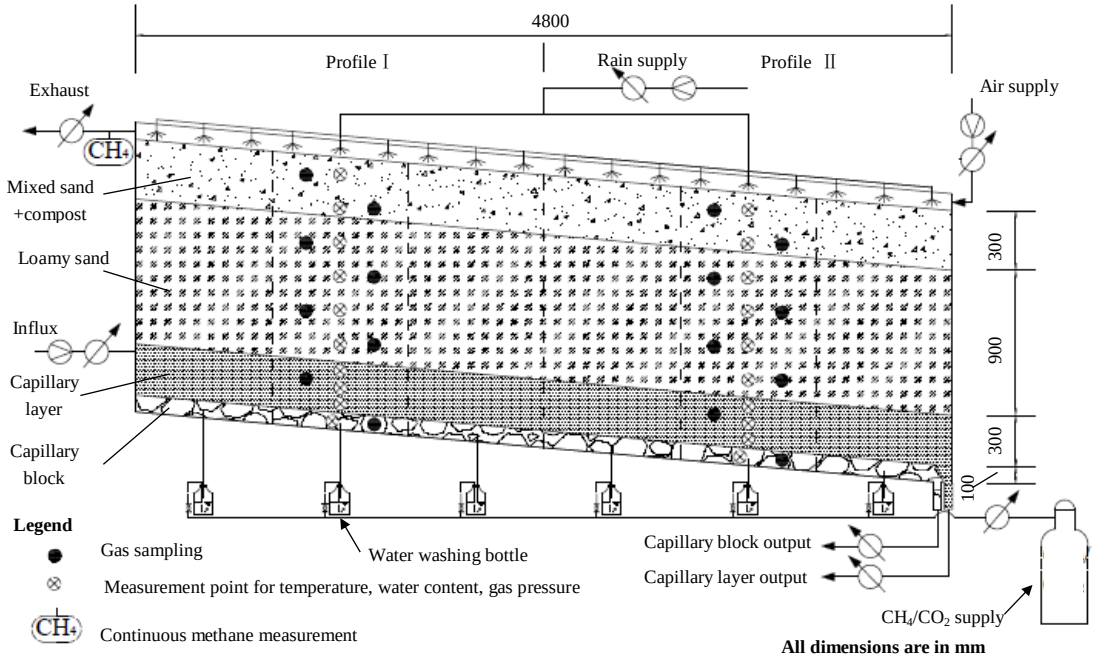

Fig. 1 Experimental flume setup for validating the 2-D numerical simulation of methane oxidation (After Berger et al., 2005)

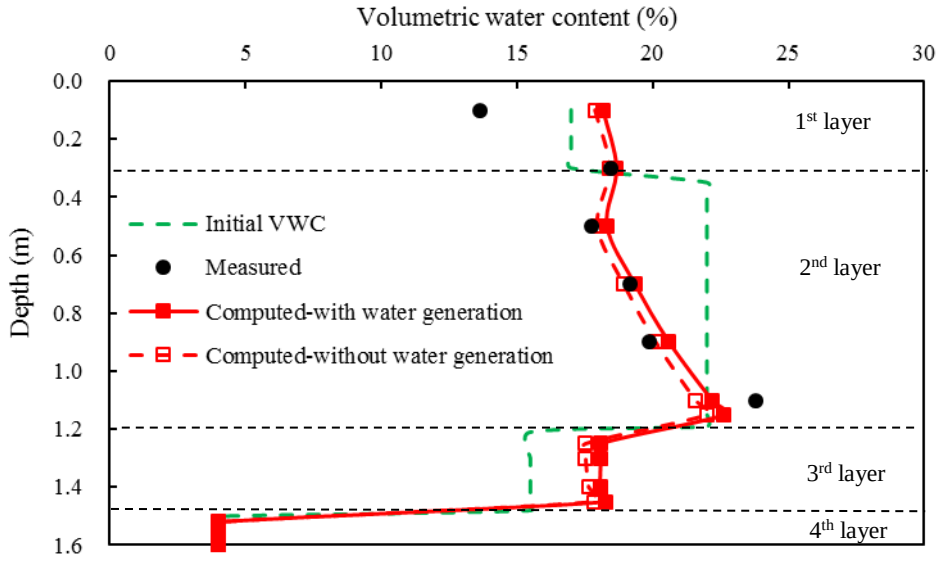

(a)

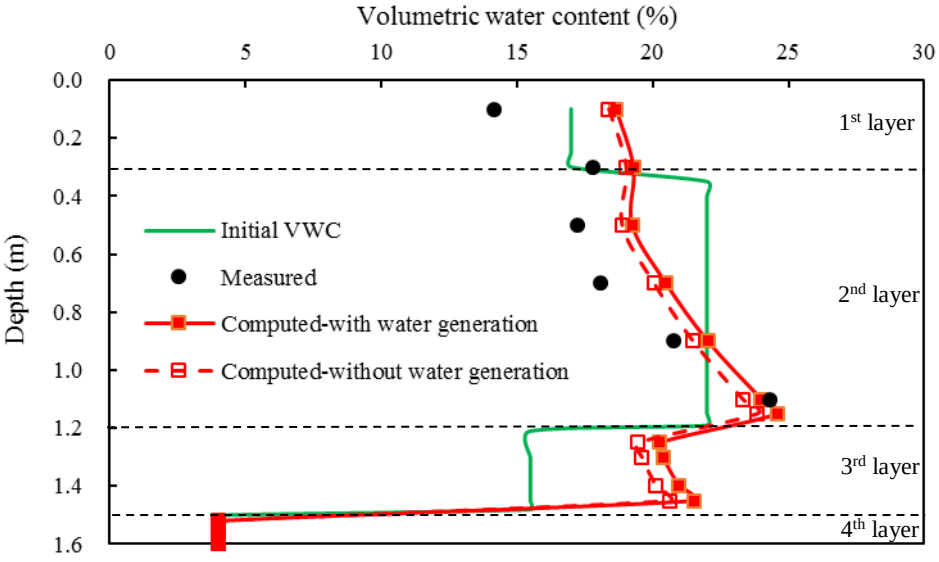

(b)

Fig. 2 Comparisons between measured and computed volumetric water contents: (a) at profile I; and (b) at profile II with and without considering water generation by methane oxidation

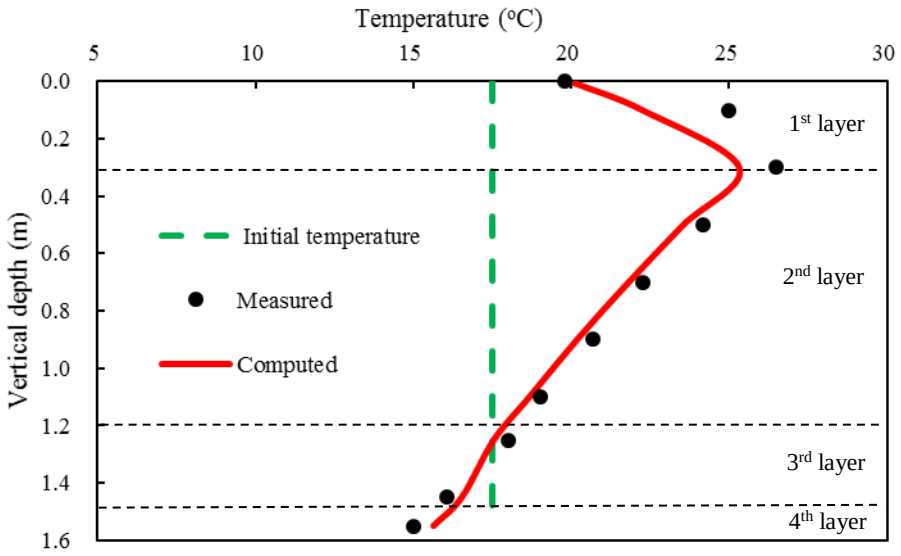

(a)

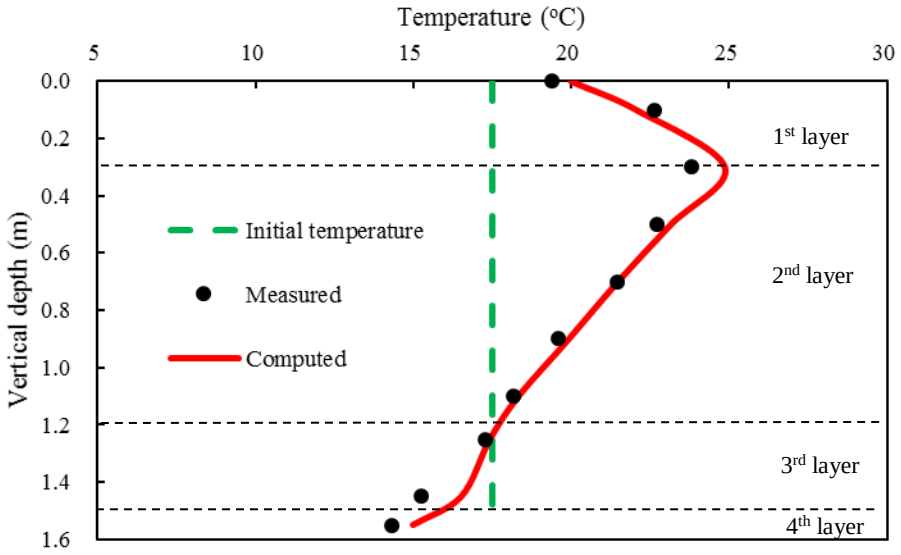

(b)

Fig. 3 Comparisons between measured and computed temperatures: (a) at profile I; and (b) at profile II

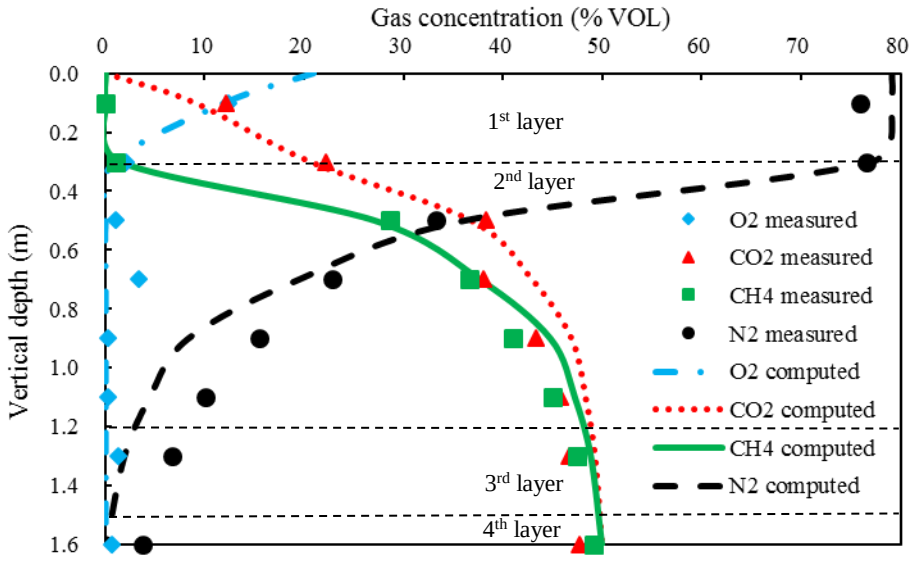

(a)

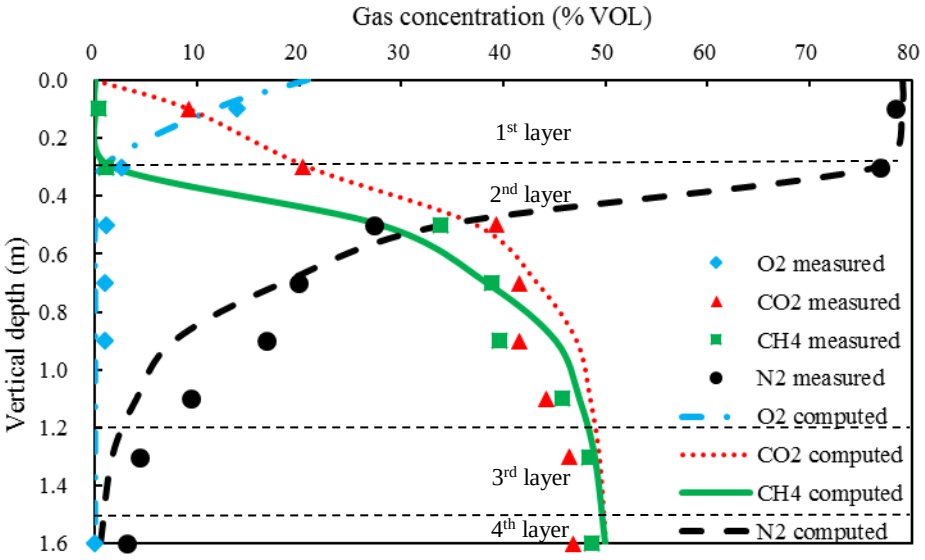

(b)

Fig.4 Comparisons between measured and computed concentrations of different gases: (a) at profile I; and (b) at profile II

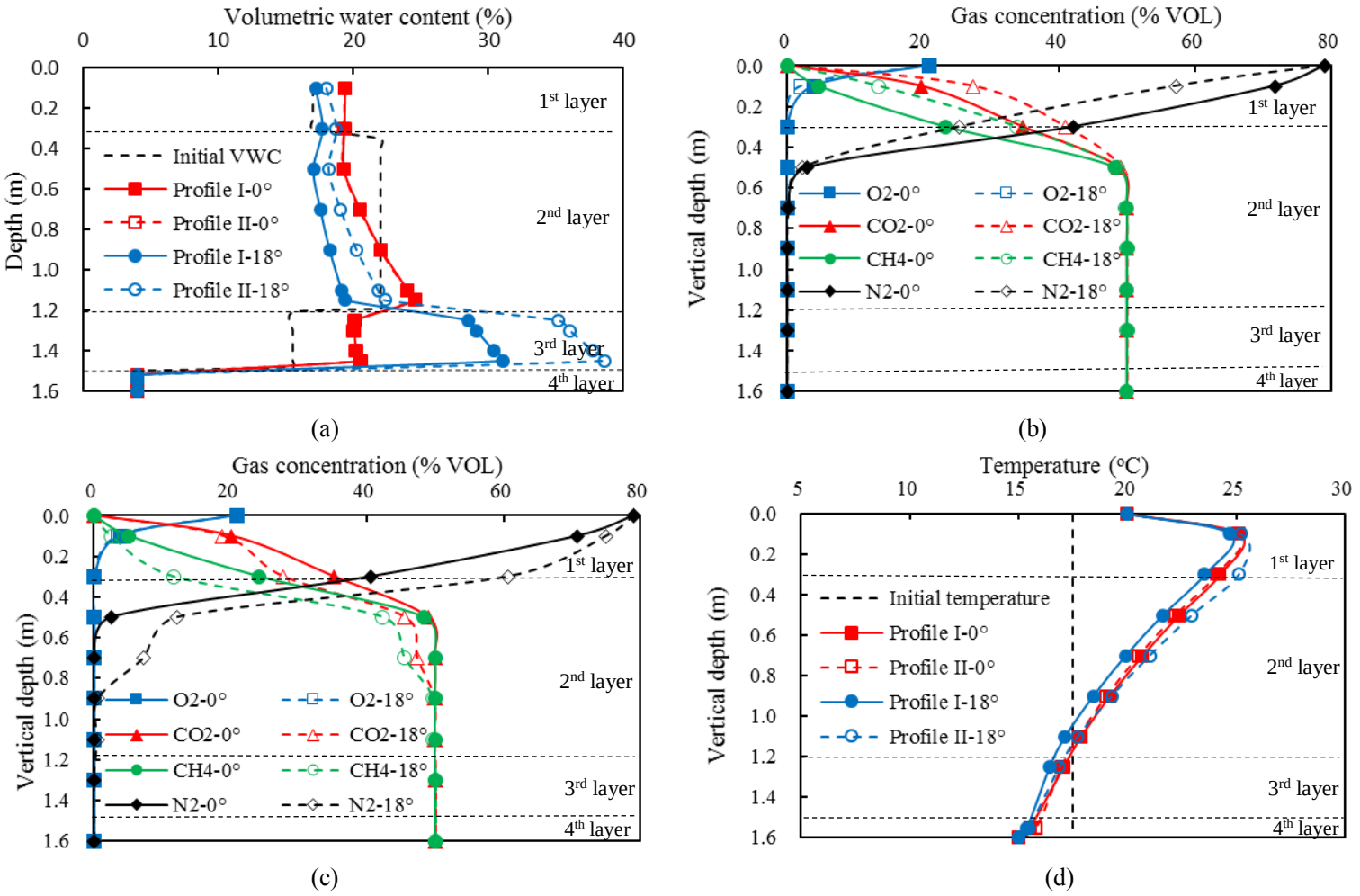

Fig. 5 Comparison of computed results at cover angles of 0° and 18°: (a) volumetric water content; (b)gas concentration at profile I; (c) gas concentration at profile II; and (d) soil temperature

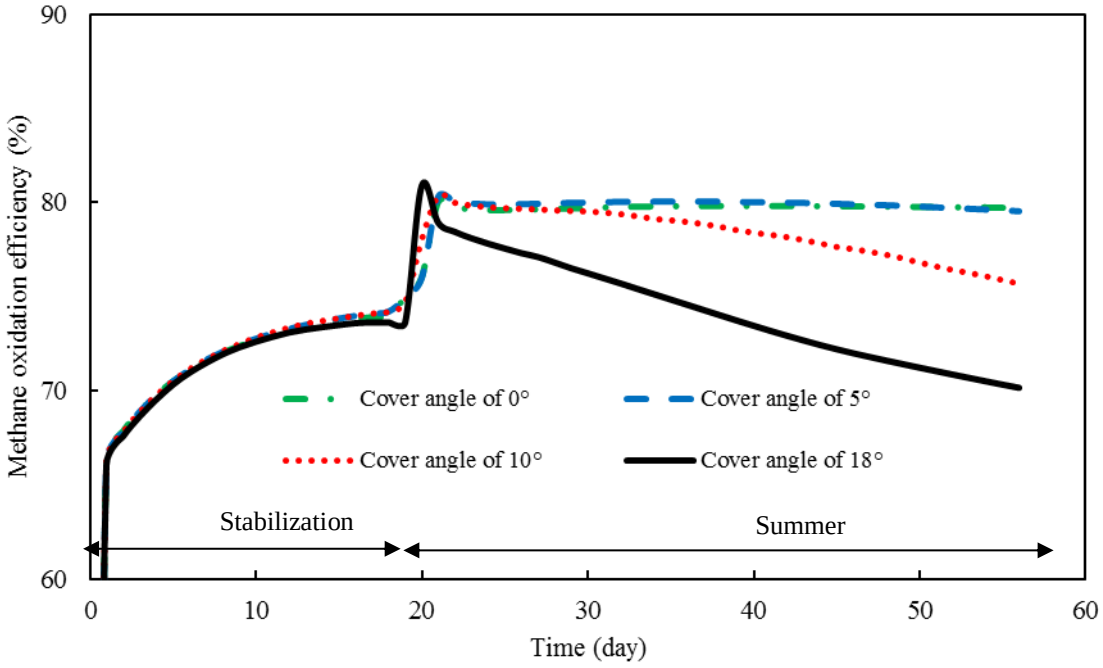

Fig. 6 Influence of landfill cover angle on methane oxidation efficiency

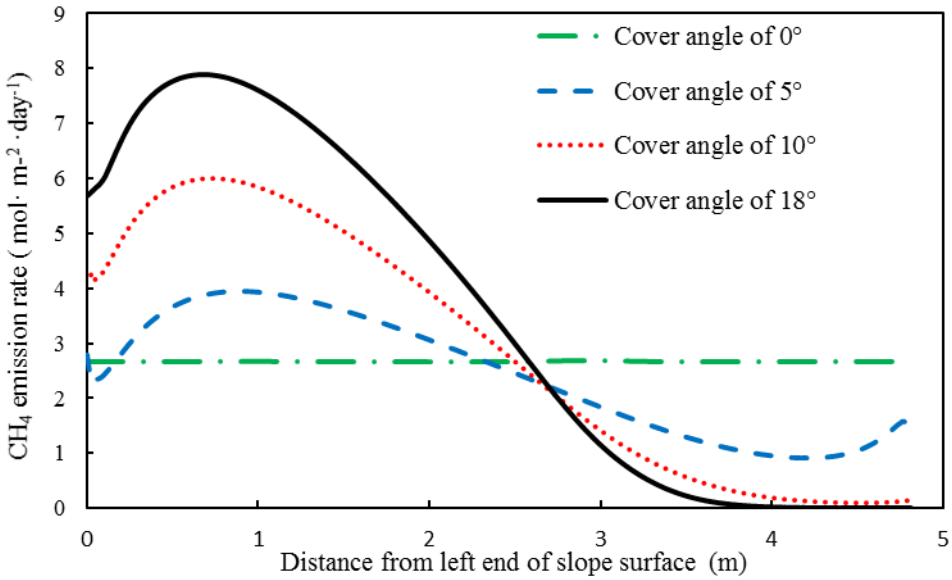

Fig. 7 Distributions of methane emission rate on the cover surface with different slope angles

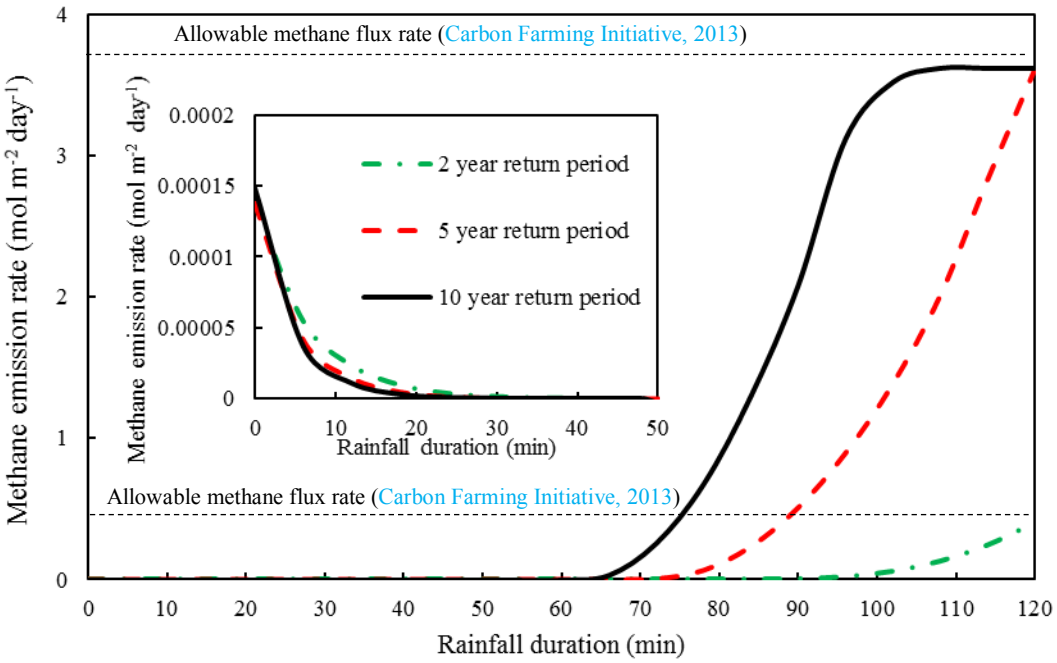
Allowable methane flux rate (Carbon Farming Initiative, 2013)
Methane emission rate (mol m-2 day-1)
Rainfall duration (min)
2 year return period
5 year return period
10 year return period
Allowable methane flux rate (Carbon Farming Initiative, 2013)
Methane emission rate (mol m-2 day-1)
Rainfall duration (min)

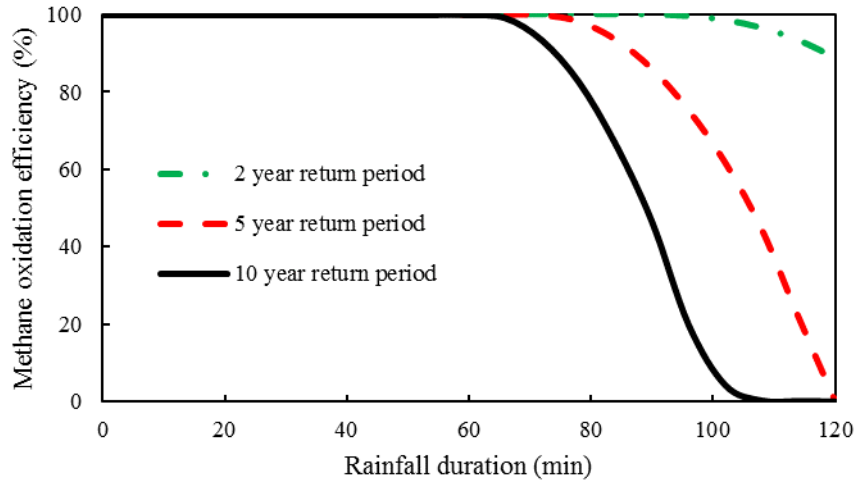

(a)

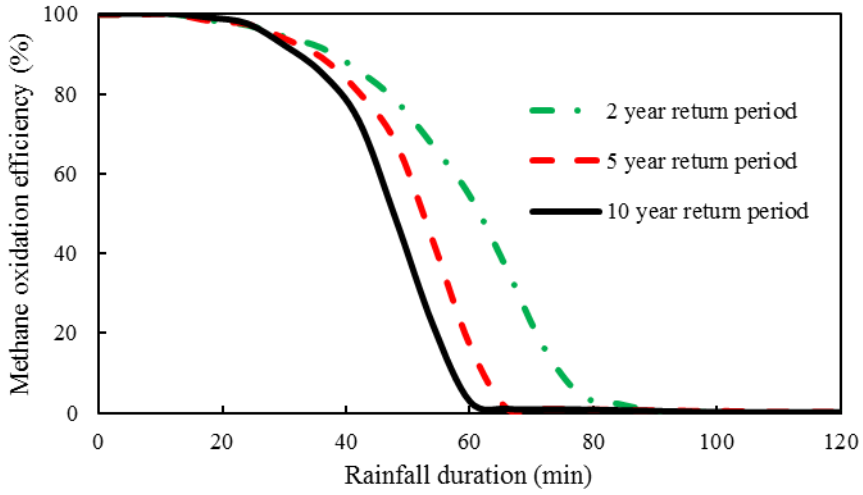

(b)

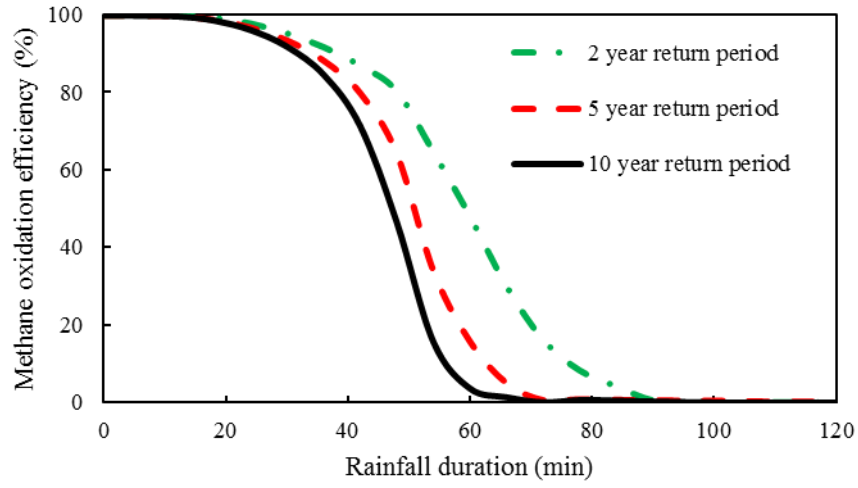

(c)

Fig. 9 Influence of rainfall intensity on methane oxidation efficiency estimated by (a) the traditional method (Eq. (14)); (b) the newly-modified method (Eq. (18)); and (c) the alternative method (Eq. (19))

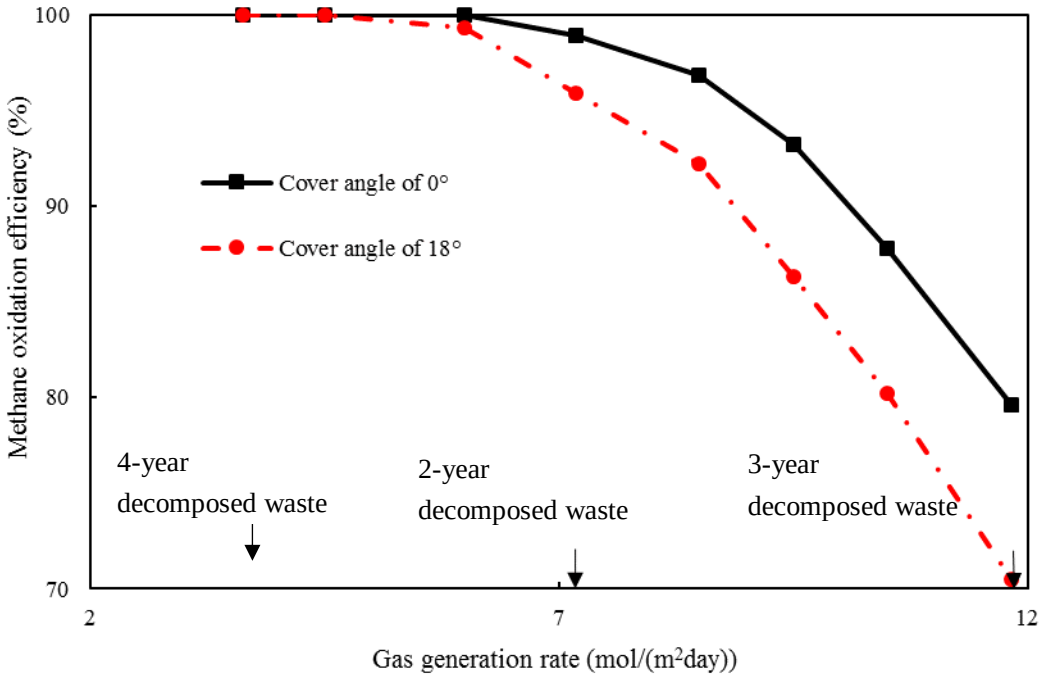

Fig. 10 Influence of gas generation rate on methane oxidation efficiency at cover angles of 0° and 18°

Supplementary Material

Numerical modelling of methane oxidation efficiency and coupled water-gas-heat reactive transfer in a sloping landfill cover

S. Feng, C. W. W. Ng, A.K. Leung and H.W. Liu*

Department of Civil and Environmental Engineering, Hong Kong University of Science and Technology, Clear Water Bay, Kowloon, Hong Kong

* (Corresponding author) **Address:** Department of Civil and Environmental Engineering, Hong Kong University of Science and Technology, Clear Water Bay, Kowloon, Hong Kong **E-mail:** hliuan@connect.ust.hk **Tel.:** +852 6849 4779

The supplementary material includes:

Part 1 Determination of diffusion coefficient in unsaturated soil

Diffusion coefficient is determined as follows (Ng et al., 2015):

$$D_s^k = \tau D_g^k \tag{S1}$$

where τ is the relative diffusion coefficient incorporating the effect of a reduced cross-sectional area and an increased path length in the presence of solid and liquid obstacles (Jin and Jury, 1996). D_g^k is molecular diffusion coefficient of gas *k* in a free gas mixture containing m gas components and is given as (Reid et al., 1987)

$$D_g^k = \frac{(1-y_k)}{\sum_{\substack{j=1 \\ j\neq k}}^{4} \frac{y_j}{D_{kj}}} \tag{S2}$$

where D_{ij} is diffusion coefficient of the binary mixture of gases *i* and *j*.

The correction factor τ is given by Millington (1959)

$$\tau = \frac{[(1\text{-}S_w)\phi]^{10/3}}{\phi^2} \tag{S3}$$

Part 2 Effects of temperature and water content on microbial activity

The effects of temperature on microbial activity ($f_{V,T}$) may be described by the following empirical expression proposed by Abichou et al., (2011):

$$f_{V,T}=\begin{cases}2.235-0.18(T-33) & T\geq 33\ ^{0}\mathrm{C}\\ 0.122T-1.47 & 15\ ^{\circ}\mathrm{C}\leq T<33\ ^{0}\mathrm{C}\\ 0.0142T & T<15\ ^{0}\mathrm{C}\end{cases} \quad \text{(S4)}$$

The physical meaning of Eq. (S4) is that below the optimum temperature of 33 ^{o}C, the rate of methane oxidation increases with an increase in temperature, but it is the opposite when soil temperature is higher than the optimum value. According to Abichou et al. (2011), the effects of soil water content on microbial activity ($f_{V,m}$) may be described by the following relationship:

$$f_{V,m}=\begin{cases}0 & \theta_{w}\leq\theta_{wilting}\\ \dfrac{\theta_{w}-\theta_{wilting}}{\theta_{fc}-\theta_{wilting}} & \theta_{wilting}<\theta_{w}\leq\theta_{fc}\\ 1 & \theta_{fc}<\theta_{w}\leq\theta_{saturated}\end{cases} \quad \text{(S5)}$$

where $\theta_{saturated}$ is saturated volumetric water content; $\theta_{wilting}$ is wilting point of soil, which is the water content when microbial activity for methane oxidation is negligible; and θ_{fc} is field capacity of soil, and it is defined as the water content at which a soil can hold when drainage driven by gravity is negligible. Eq. (S5) describes that when soil water content is lower than $\theta_{wilting}$, methane oxidation is negligible. As soil water content increases from $\theta_{wilting}$ to θ_{fc}, methane oxidation rate increases linearly to the maximum value. When the water content is higher than field capacity, $f_{V,m}$ becomes constant, meaning that the soil water content has no effect on microbial activity.

Part 3 Extra figures

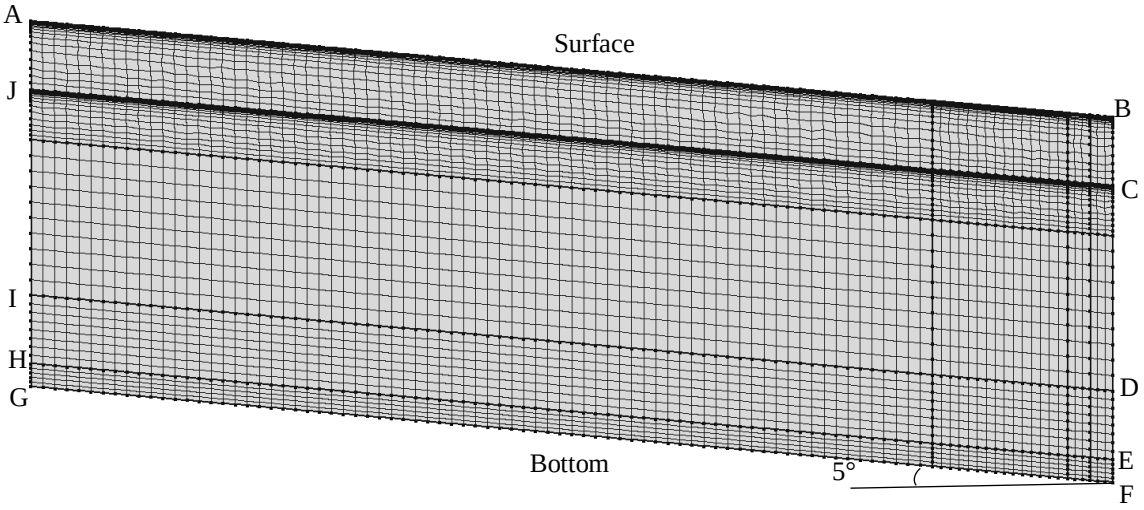

Fig. S1 Finite element mesh adopted for two-dimensional simulation

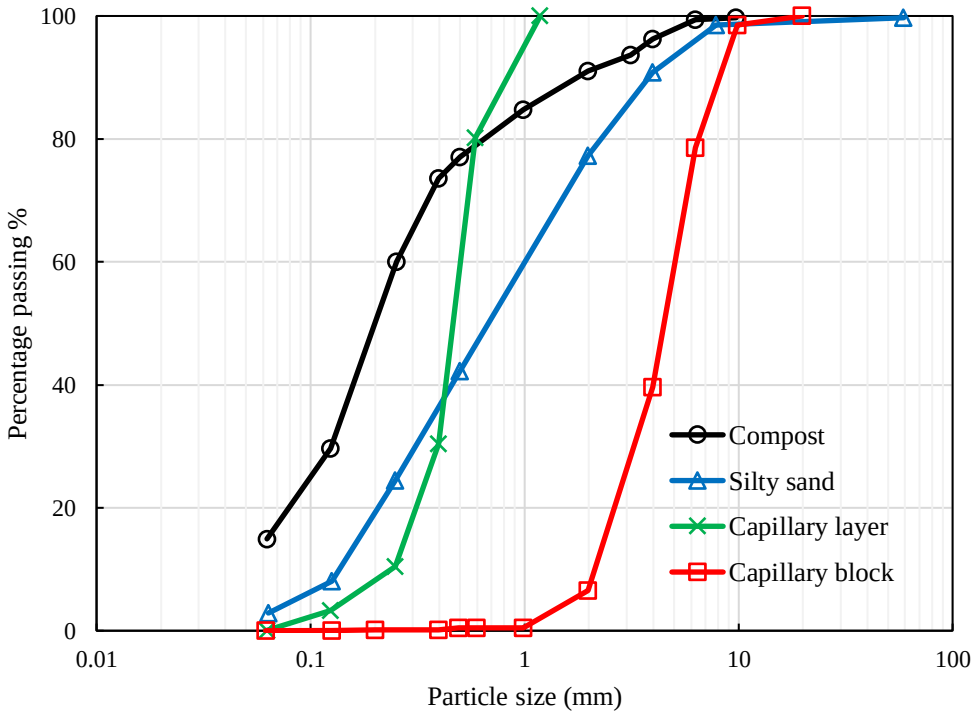

Fig. S2 Particle-size distributions for different soils (After Berger, 2008)

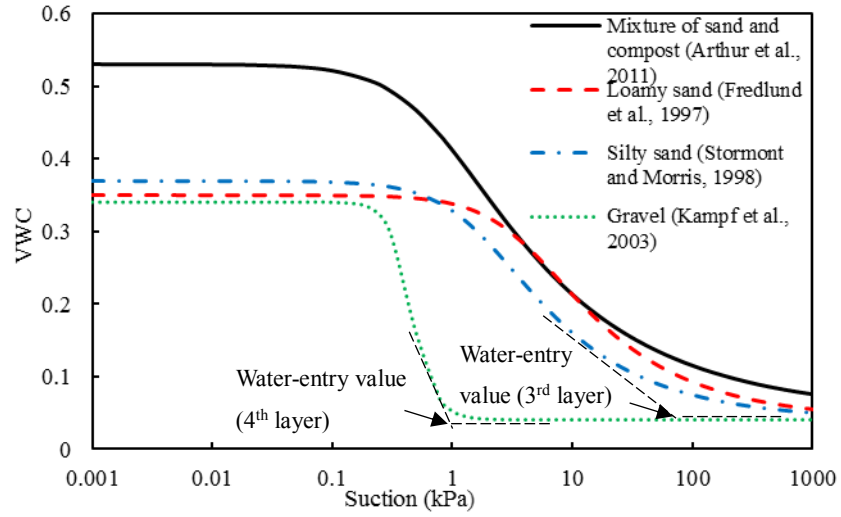

(a)

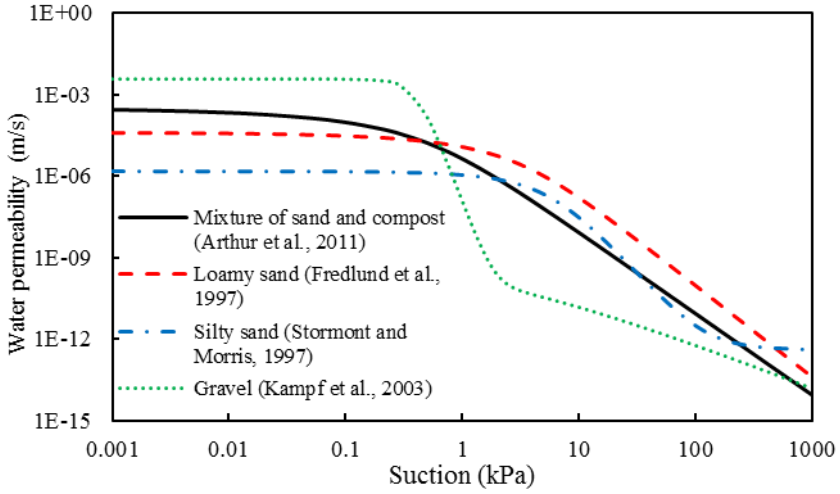

(b)

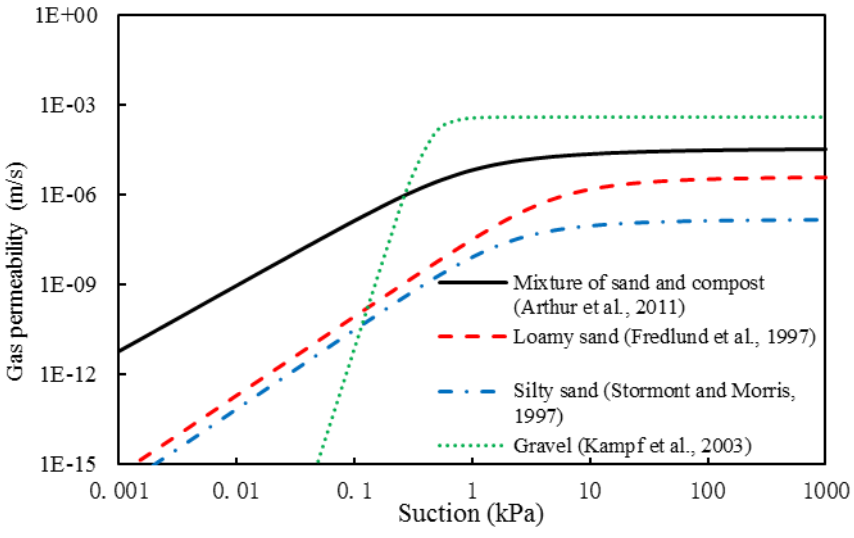

(c)

Fig. S3 Hydraulic parameters adopted for different soils: (a) SWCCs; (b) water permeability functions; (c) gas permeability functions

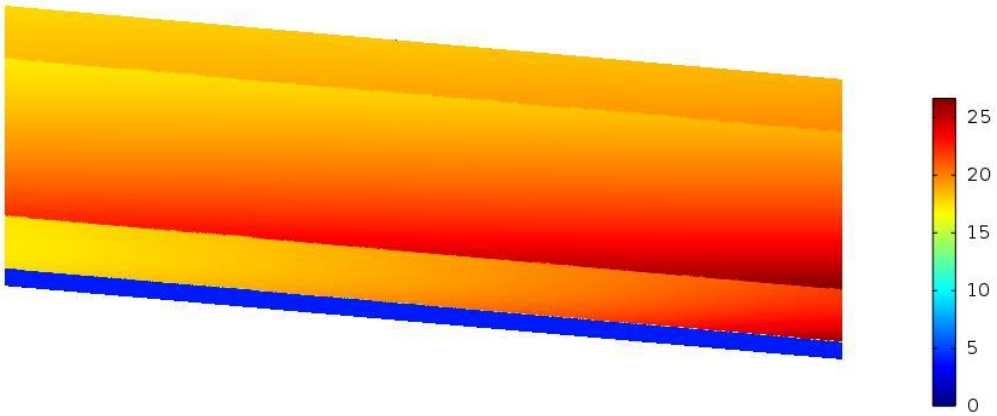

Fig. S4 Computed contour of volumetric water content (%) on Day 56

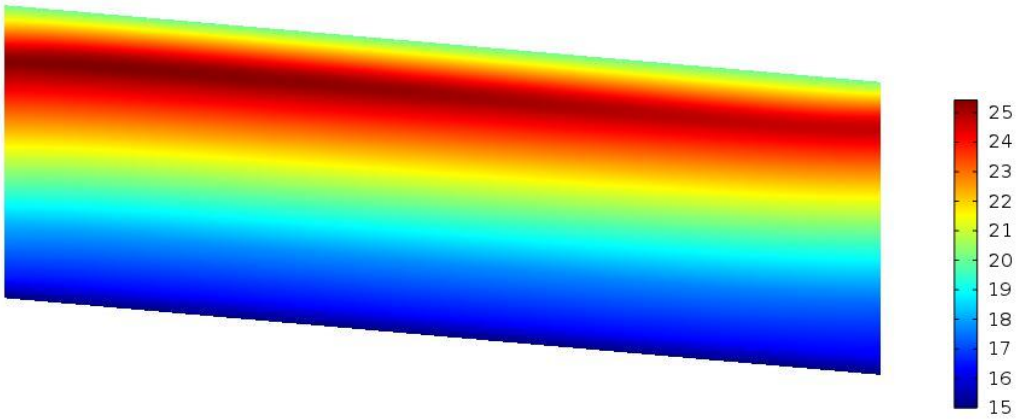

Fig. S5 Computed contour of temperature (°C) on Day 56

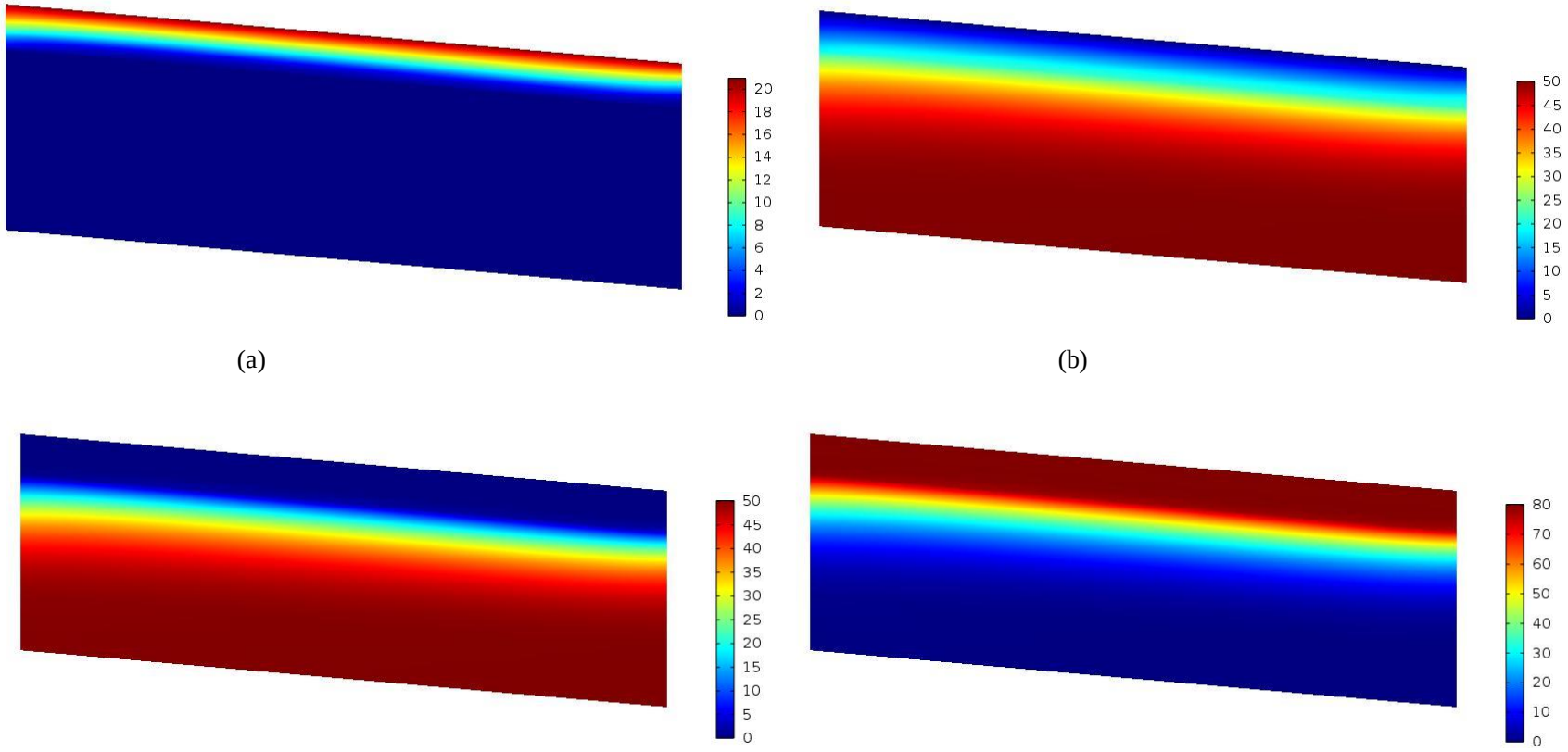

Fig. S6 Computed contour of gas concentration (%) of (a) O_2; (b) CO_2; (c) CH_4; and (d) N_2 on Day 56

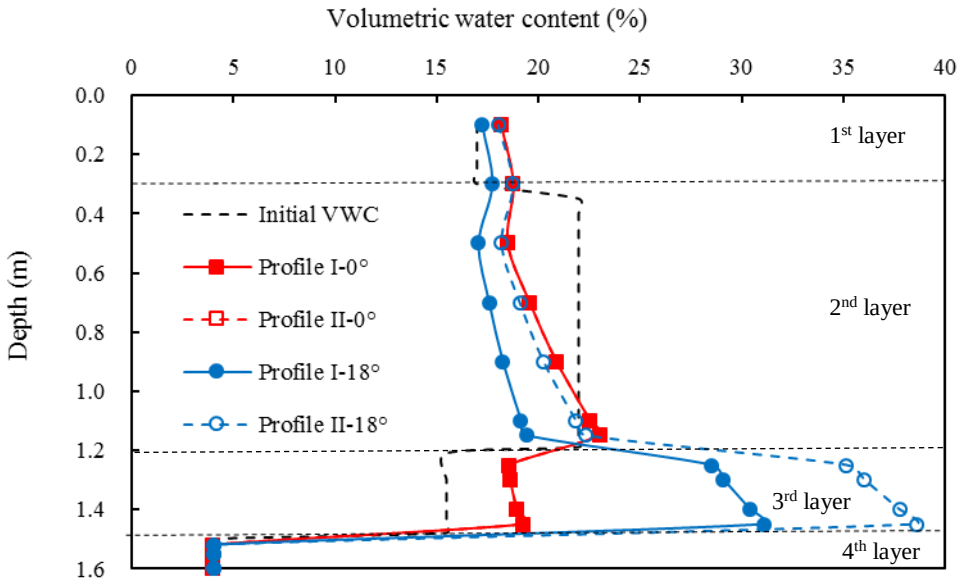

Fig. S7 Comparison of computed volumetric water content distributions without considering water generation by methane oxidation at cover angles of 0° and 18°

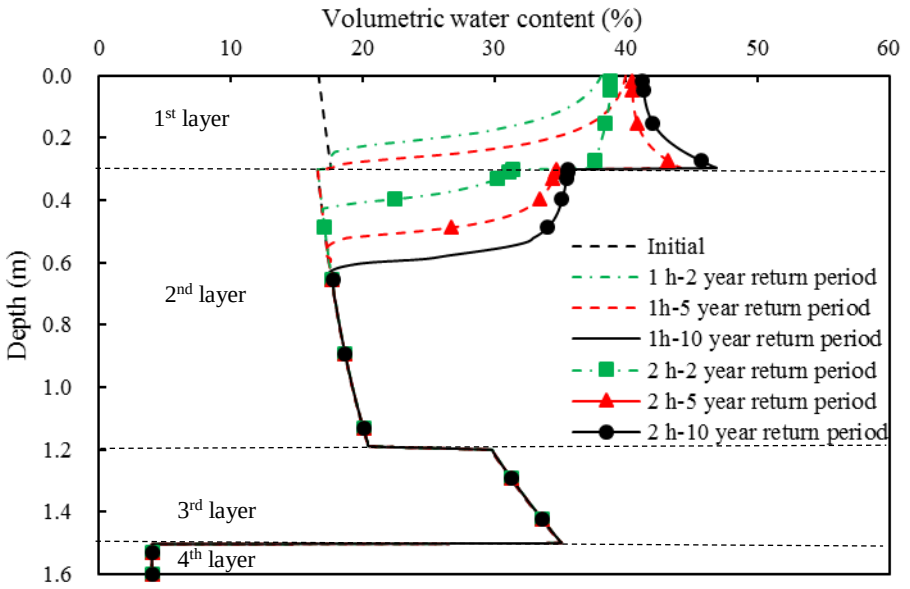

(a)

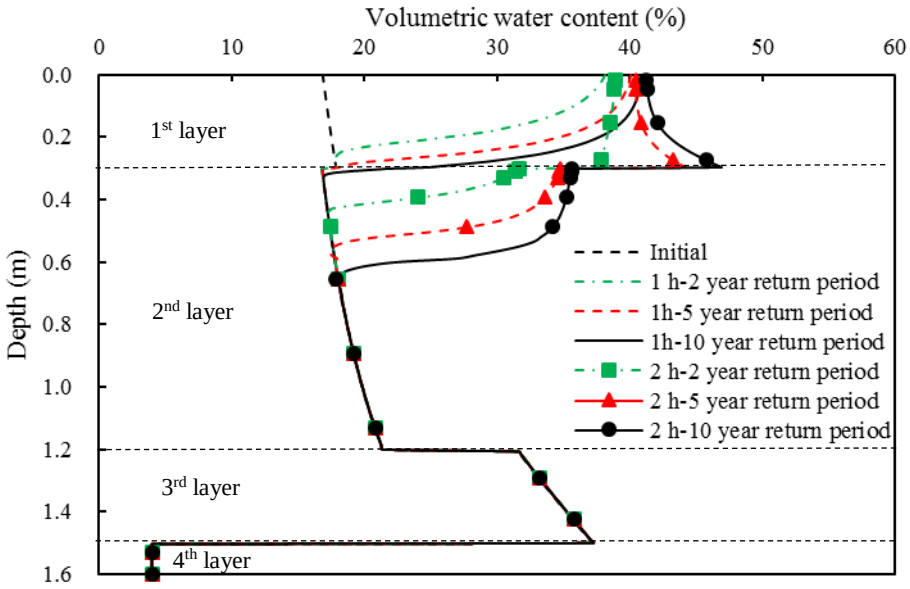

(b)

Fig. S8 Computed volumetric water content distributions during different rainfall intensities: (a) at profile I; and (b) at profile II

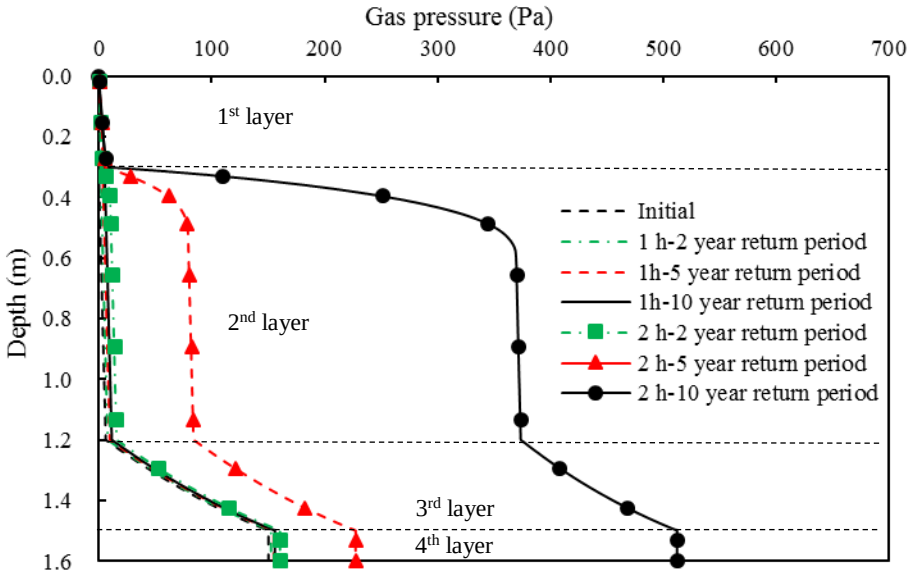

(a)

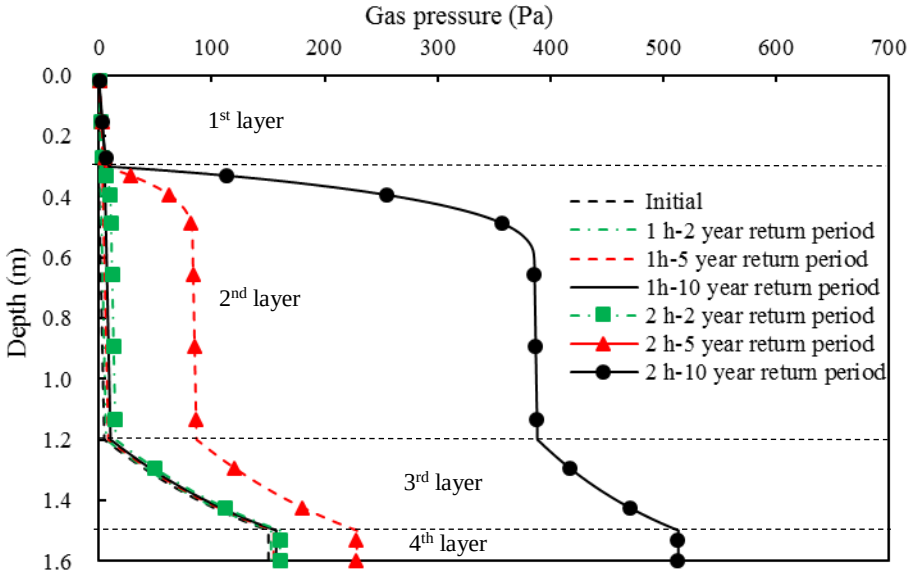

(b)

Fig. S9 Computed gas pressure distributions during different rainfall intensities: (a) at profile I; and (b) at profile II

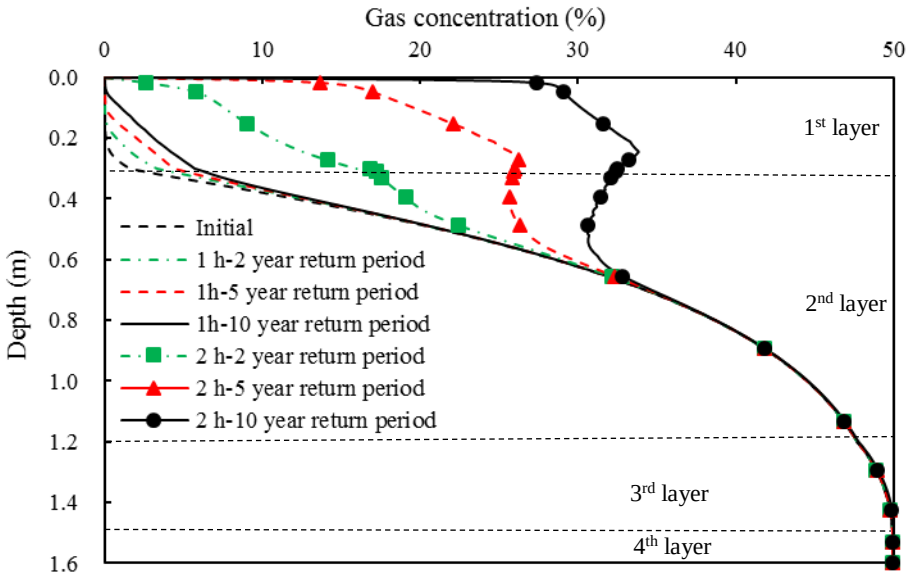

(a)

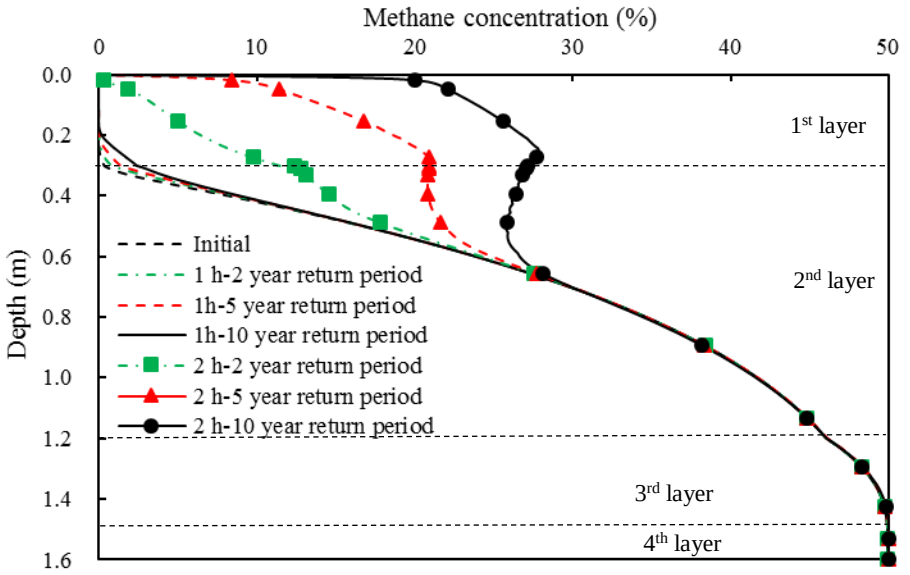

(b)

Fig. S10 Computed methane concentration distributions during different rainfall intensities: (a) at profile I; and (b) at profile II

References

Abichou, T., Mahieu, K., Chanton, J., Romdhane, M. and Mansouri, I., 2011. Scaling methane oxidation: from laboratory incubation experiments to landfill cover field conditions. Waste Management, 31, 978–986.

Jin, Y. and Jury, W. A., 1996. Characterizing the dependence of gas diffusion coefficient on soil properties. Soil Science Society of America Journal, 60(1), 66-71.

Millington, R.J., 1959. Gas diffusion in porous media. Science, 130, 100-102.